Spring 5-7-2016

Color Stability, Physical Properties and Antifungal Effects of ZrO2 and TiO2 Nanoparticle Additions to Pigmented Polydimethylsiloxanes

Mazen Alkahtany
University of Nebraska Medical Center

Color Stability, Physical Properties and Antifungal Effects of ZrO_2 and TiO_2 Nanoparticle Additions to Pigmented Polydimethylsiloxanes

By

Mazen Alkahtany

A THESIS

Presented to the Faculty of

The University of Nebraska Graduate College

In Partial Fulfillment of the Requirements

For the Degree of Master of Science

Medical Sciences Interdepartmental Area

(Oral Biology)

Under the Supervision of Professor Mark Beatty

University of Nebraska Medical Center

Omaha, Nebraska

May, 2016

Advisory Committee:

Fahd Alsalleeh Ph.D.

Dennis Feely Ph.D.

Thomas M. Petro Ph.D.

You Zhou Ph.D.

ACKNOWLEDGMENTS

First of all, I would like to express my sincere gratitude to my advisor Dr. Mark Beatty for the continuous support of my Master study and related research, for his patience, motivation, and immense knowledge. His guidance helped me in all the time of research and writing of this thesis.

My completion of this project could not have been accomplished without the support of the rest of my committee members: Dr. Fahd Alsalleeh during his time as the postgraduate endodontic program director, Dr. Thomas Petro, Dr. Dennis Feely and Dr. You Zhou. I would like to thank them for their insightful comments and inspiration.

I cannot express enough thanks to Bobby Simetich. His invaluable experience in the materials lab and his support all the time of my study were a great help to complete this thesis.

My sincere thanks also go to all faculty, staff, lab members and instructors for your support, friendship and encouragement. Also I thank my friends in the University of Nebraska Medical Center for all the support and time we have been sharing.

I would like to thank my family: My dad who planted the seed of ambition in me to fulfill my dream and come to the great country of the United States of America. Mom, who continuously supported, encouraged and helped me keep a level head during my studies home and in the United States.

Last but not least, thank you to my wife for supporting me and living my residency and studies with me throughout our stay in the great state of Nebraska where we were blessed with our two wonderful babies, Wasn and Faisal.

Color Stability, Physical Properties and Antifungal Effects of ZrO_2 and TiO_2 Nanoparticle Additions to Pigmented Polydimethylsiloxanes

Mazen Alkahtany B.D.S., M.S.

University of Nebraska Medical Center, 2016

Advisor: Mark W. Beatty, D.D.S., M.S.E., M.S.D., M.S.

Introduction: Color changes, physical degradation and fungal infections are potential challenges to the longevity of polydimethylsiloxane (PDMS) elastomers. The purpose of this study was to evaluate potential improvements in color change, physical properties and antifungal properties of PDMS loaded with TiO_2 and ZrO_2 nanoparticles.

Methods: 1% weight of 40 nm or 200 nm diameter TiO2 or ZrO_2 nanoparticles were mixed into PDMS with 2% functional intrinsic yellow pigment and polymerized. Control materials contained 13% weight 200 nm silica. Samples were exposed to either 3000 hours of UVB radiation (200 $\mu W/cm^2$) or darkness. Color parameters L*a*b* and ΔE^*, ultimate tensile strength, strain, elastic modulus and shore A hardness were measured. Data were analyzed using a factorial ANOVA with Tukey-Kramer *post hoc* test ($p<0.05$). *Candida albicans* growth was measured using XTT and confocal microscopy and data analyzed with the Dunnett test ($p<0.01$).

Results: TiO_2 200 nm showed the least color change after 3000 hours of UVB weathering, followed by TiO_2 30-40 nm ($p<0.05$). The silica control group was superior in all physical property measurements ($p<0.05$). TiO_2-containing materials exhibited statistically significantly lower *C. albicans* growth ($p<0.01$).

Conclusion: 40 nm and 200 nm TiO_2 nanoparticles, when added to pigmented PDMS at 1% weight, provide improved color stability and lower *C. albicans growth* compared to silica- and zirconia-filled elastomers.

TABLE OF CONTENTS

LIST OF FIGURES

LIST OF TABLES

LIST OF ABBREVIATIONS

a*	Red-green axis of CIE L*A*B* system
AAA	American Association of Anaplastology
AAMP	American Academy of Maxillofacial Prosthetics
ANOVA	Analysis of variance
ASTM	American Society for Testing of Materials
ATP	Adenosine triphosphate
b*	Yellow-blue axis of CIE L*A*B* system
C.albicans	*Candida albicans*
CA42	*C. albicans* wild-type SC5314 strain
CIE L*A*B*	Comission Internationale de l'Eclairge color system
FBS	Fetal bovine serum
FUN-1	Fluorescent vital dye for yeast and fungi
L*	White-black axis of CIE L*A*B* system
PBS	Phosphate-buffered saline
PDMS	Polydimethylsiloxane
PVC	Polyvinyl chloride
PVS	Polyvinyl siloxanes
RTV	Room temperature-vulcanized silicone products
UTS	Ultimate tensile strength
UV	Ultraviolet
UVB	Ultraviolet B
Vol.%	Percentage of volume loaded
Weight. %	Percentage of weight loaded

XTT	2,3-bis (2-methoxy-4-nitro-5-sulfophenyl)-5-([phenyl amino] carbonyl)-2H-tetrazolium hydroxide colorimetric assay
YNB	Yeast nitrogen base medium
ΔE*	Overall color change

CHAPTER 1: INTRODUCTION

Extra-oral maxillofacial prostheses are essential treatment options for patients suffering significant defects of facial structures. These defects can result from trauma, disease or as a congenital anomaly, and can lead to psychological and social trauma. Patients with such defects require multidisplinary therapeutic care, involving a team effort between the maxillofacial surgeon, maxillofacial prosthodontist and reconstructive surgeon (Lemon et al., 2005), as well as follow-up psychological therapy. Prosthetic rehabilitation provides psychological and functional benefits, as it enhances aesthetics, speech, swallowing, self-esteem and overall quality of life. Studies have shown that the survival rates of head and neck cancer are improving (Carvahlo et al., 2005), thus maxillofacial prostheses are increasingly in demand.

Since 1960, silicon-based elastomers have been used to fabricate maxillofacial prostheses due to their flexible mechanical properties and translucent optical properties (Barnhart 1960). However, common clinical problems of these materials include gradual color loss and degradation of physical properties over time in a service environment (Beatty et al., 1995, Polyzois et al., 1999).

Color changes and physical properties of these elastomers are multifactorial. Mechanical loading and environmental factors such as ultraviolet exposure, temperature and relative humidity have been identified as potential challenges for an elastomer's optical and physical stability. Of these factors, ultraviolet radiation is considered a key factor in decomposing the elastomer's optical and physical properties. Another potential challenge is the susceptibility to fungal infection on the tissue side of the prosthesis (Udagama 1987).

Previous research indicated promising results with addition of nano-sized particles to silicon elastomers in terms of physical and optical properties. Nano-sized oxide particles such as

TiO_2 and ZrO_2 are characterized by their small size, large surface area and strong interactions with the organic polymer. Therefore, they can improve the optical and physical properties of the polymer, as well as its resistance to environmental stress-induced cracking and aging (Liu et al., 2005). Also, certain nanoparticles, such as silver, have been shown to provide antifungal activity. The mechanism of action is not fully understood, but biocidal and anti-adhesive activity, and delivery of antimicrobial agents such as mixed ligand-metal complexes have been suggested (Allaker 2010).

Candida albicans accounts for 70-80% of all fungal infections and is increasingly associated with biomaterial-related infections. It is part of the normal flora on skin and mucosal surfaces. Thus, it is of particular interest of this investigation to assess the antifungal effect of incorporating TiO_2 and ZrO_2 nanoparticles into the silicon elastomer.

The purpose of this thesis is to incorporate TiO_2 and ZrO_2 nanoparticles into pigmented PDMS elastomers and assess changes in color, physical and antifungal properties. The central hypothesis of this study is that adding TiO_2 and ZrO_2 nanoparticles to pigmented PDMS elastomers will improve color stability and physical properties when subjected to controlled dosages of ultraviolet radiation. The second hypothesis is that *C. albicans* growth on the surface of pigmented PDMS elastomers will be reduced by addition of TiO_2 and ZrO_2 nanoparticles. These hypotheses are tested via a set of null hypotheses stated in the following specific aims. Specific aim #1 tests the first null hypothesis that color stability of silicon elastomers will not be affected by the addition of TiO_2 and ZrO_2 nanoparticles. Specific aim #2 tests the second null hypothesis that physical properties of hardness and tensile properties of silicon elastomers will not be affected by adding TiO_2 and ZrO_2 nanoparticles. Finally, specific aim #3 tests the third null hypothesis that the antifungal activity is the same for silicon elastomers with or without TiO_2 and ZrO_2 nanoparticles.

CHAPTER 2: LITERATURE REVIEW

2.1 Maxillofacial Prostheses History and Characteristics.

Maxillofacial materials are used to replace missing facial parts that have been lost through trauma, disease or congenital anomaly. Throughout history several materials have been used to replace missing parts of the maxillofacial region including wood, ivory, waxes, and metals (Andres et al., 1992). Kazanjian et al., (1932) described painting a vulcanite rubber to match the color of the skin. Other materials have included latex, poly (methyl-methacrylate), vinyl chloride polymers, polyurethane, acrylic resin and silicone (Bulbulian 1942, Chalian et al., 1974). In the 1960's poly (siloxane) rubber materials were introduced in the maxillofacial prosthetic technology by Barnhart. Since then these elastomers have been the material of choice for the fabrication of maxillofacial prosthesis. Nowadays, silicon-based elastomers are the materials of choice in the field of maxillofacial prosthetics, specifically polydimethyl siloxane (PDMS) (Aziz et al., 2003). A 2010 survey showed that the majority of the American Association of Anaplastology (AAA) and American Academy of Maxillofacial Prosthetics (AAMP) members were using room temperature-vulcanized (RTV) silicone products (Kiat-Amnuay et al 2010).

Cantor et al. in 1969 suggested a method to evaluate prosthetic materials in response to the rising need at that time for an objective, scientific and reproducible method for evaluating color of facial prostheses. This method utilized spectrophotometric curves and it was determined that facial materials could be isometrically matched to human skin color. With the emergence of new materials and techniques in the field of maxillofacial prosthesis, the development of a specification was essential. In 1972 Sweeny et al. developed the Sweeney specification by analyzing mechanical properties of polymerized poly (vinyl chloride). A specification table was presented and included hardness, strength, elastic modulus, tear

strength and chemical stability under weathering conditions using a weatherometer. In 1974 Lontz et al., found that polysiloxanes properties can be improved through modification with oils and crosslinking agents to approximate the stress-strain profiles of human aorta and tendons. The rationale behind this approach was that in order for maxillofacial materials to simulate oral tissues, the dynamic nature of these tissues must be considered, as they are constantly moving and are exposed to tensile and compressive forces. It was argued that laboratory tests for elastomers should include both static and dynamic properties, since their stress-strain behavior is non-linear and they undergo time-dependent strain (Lontz et al., 1968, Craig & Koran 1975).

In an effort to improve physical properties of maxillofacial prosthetic materials, mixing of different compounds has been attempted in order to combine desired properties of each component into the end result. In a study conducted by Firtell et al., room temperature vulcanized (RTV) silicone was mixed with foam RTV silicone to lower its density and weight. The resulting material demonstrated a reduced weight but exhibited a shorter clinical life due to loss of tear strength. Another approach was to modify the polymer-to-crosslinking agent ratio. This was accomplished with polyurethane and proved that physical and mechanical properties such as surface hardness, modulus of elasticity, strength and strain can be improved (Gonzales et al., 1978 and Goldberg et al., 1978). Other studies used the concept of adding reinforcing fillers such as nylon, glass fiber, silica fibers and tulle. These additions produced a rigid and heavy composite material that had improved marginal tear resistance (Karayazgan et al., 2003 & Gunay et al., 2008).

One of the most critical properties of a maxillofacial prosthesis is color stability. Craig and his group were one of the first to test the color stability of facial elastomers using an artificial weathering approach (Craig et al., 1978). In this study, color stability of polyvinyl

chloride, polyurethane and silicone elastomers for maxillofacial applications was determined after artificial weathering, using reflectance spectrophotometry. Measured parameters were luminous reflectance, contrast ratio, dominant wavelength and excitation purity, which were calculated using a computer program based on the C.I.E L*a*b* (Commission Internationale de l'Eclairge) color system. Luminous reflectance is a measure of the total amount of light reflected by the specimen and is a measure of lightness or darkness. Contrast ratio is the ratio of luminous reflectance with a black to a white background. Dominant wavelength is the actual color of the specimen when compared to a standard observer and is similar to hue. Excitation purity is a measure of the amount of color present in the sample and is similar to chroma. Their results showed that silicone elastomers were the most promising in terms of color stability compared to the other two materials after 900 hours of artificial weathering.

Although elastomers show excellent aesthetics initially, color stability is a significant challenge. A survey study found that 70% of maxillofacial prosthetic patients had their appliances remade within one year, of which 29% were due to color change (Jani and Schaaf 1978). Other studies have reported that the clinical service lifetime of a prosthesis is usually 6 months to 2 years, with an average of 10 months (Jani and Schaaf 1978, Chen et al., 1981 and Polyzois 1999).

Ideally a maxillofacial prosthesis should possess high tear strength, tensile strength and toughness, high flexibility, similar hardness to surrounding tissues, low water sorption and good surface wettability (Aziz et al., 2003b, Han et al., 2008). Tear strength is especially important, particularly at the thin margins surrounding nasal and eye prostheses. In order to mask the presence of a facial prosthesis it has to be fabricated with thin margins. When a prosthesis is peeled away from facial tissues, it is subjected to tearing at its thin margins; consequently it is

important to use a material with high tear resistance. Another property to consider is flexibility. As the material is peeled away from nasal tissues it has to elongate enough before it breaks. Other important characteristics include ease of application, retention, color stability, durability, lack of toxicity, ease of cleansing, ease of fabrication and physical and chemical inertness (Yu et al., 1978).

One of the most serious problems faced by maxillofacial prosthesis is infection of the material surface by *Candida albicans* and other candida species related to denture stomatitis and gastrointestinal and pneumopulmonary candidiasis (Udagama, 1987; Pingo et al., 1994). *C. albicans* are opportunistic fungi that are part of the normal flora of the skin, oral cavity, gastrointestinal tract and urogenital tract. However, candidal infection may occur when host defenses are lowered by local factors (such as prosthesis irritation, xerostomia), medication (antibiotics, immunosuppressant drugs), chemotherapy, radiation therapy and systemic disorders (such as endocrine and immune disturbances). *C. albicans* is responsible for about 70-80% of all fungal infections (Hay, 1999). *C. albicans* are also associated with infections of biomaterials such as maxillofacial prostheses, catheters, dentures, heart valves, implanted devices and contact lenses (Ramage et al., 2001). Biofilm formation is critical in the development of candidiasis and *C. albicans* biofilms are potentially highly resistant to the currently used antifungal agents (Chandra et al., 2003). *C. albicans* in biofilm can be 100-fold more resistant to fluconazole and 30-fold to amphotericin B agents than planktonic cells (Kumamoto 2002).

Poly dimethylsiloxane (PDMS) currently is the most commonly used elastomer for maxillofacial prosthesis. Two main types of systems are used. One is room temperature vulcanizing (RTV), in which PDMS terminated with hydroxyl groups undergoes polycondensation in the presence of tin as a catalyst. The second is a heat-cured system in which unsaturated

vinyl- terminated polysiloxanes undergo free radical addition with the aid of a platinum catalyst (Aziz et al., 2003a).

Key factors affecting mechanical properties of an elastomer include molecular weight distribution, the incorporation of hydrophobic filler particles with low sizes and high surface areas, and the degree of cross-linking between polymer chains. Strategies such as the formation of bimodal networks from blending long and short chains of the same polymer can result in a combination of desired mechanical properties, such as high tear strength and flexibility (Shah & Winter 1996, Bellamy et al., 2003).

Recently interest has been gained in incorporating nanoparticles into maxillofacial prosthetic materials. Due to their high surface energy and chemical reactivity, nano-oxides tend to agglomerate in solution and can be difficult to disperse (Goiato et al., 2010). When the elastomer is subjected to external forces, the agglomerated nanoparticles act as stress-concentrating centers within the silicon matrix, thereby lowering mechanical properties and affecting dimensional stability over time (Han et al., 2008). However, when nanoparticles are properly dispersed, physical and mechanical properties of the elastomer should be improved and resistance against environmental stress cracking and aging should be gained (Lue et al., 2005).

2.2 Factors Affecting Prosthesis Degradation.

Considering that a maxillofacial prosthesis undergoes several steps of fabrication and color matching in the clinic and laboratory, a single prosthesis can become very costly to the patient. Therefore, the long-term durability of a maxillofacial prosthesis becomes extremely important. The overall deterioration of a maxillofacial prosthesis has been attributed to certain environmental factors such as exposure to the natural sunlight (specifically the ultraviolet

component), wetness and dryness of the elastomer, and surface abrasion during application and removal of the appliance (Keyf 2002).

Aging and deterioration of an extra-oral prosthesis is accompanied by increase in stiffness and loss of flexibility, leading to tearing along esthetical thin margins. Ultraviolet radiation, which enhances cross-linking and increases breaking down of the polymer, ultimately decomposes the elastomer (Hatamleh & Watts 2010). Air pollution also has been shown to affect silicone color (Mohite et al., 1994).

As stated, ultraviolet (UV) radiation is a key environmental factor that has a large impact on the optical and mechanical properties of a maxillofacial prosthesis (Beatty et al., 1999, Mohite et al., 1994, Han et al., 2010). UV photons in the presence of oxygen lead to photo-oxidative degradation of the elastomer. Energetic photons or particles (gamma rays, protons, electrons), with energy greater than the molecular bond strength, degrade the polymer through a process called radiolysis (Cottin et al., 2000). The absorption of UV photons leads to degradation of the molecule and the production of smaller polymer chains and volatile degradation products. Due to the presence of free radicals, a competition occurs among initiation, propagation and termination (Rabek 1995). This polymerization disturbance produces changes within the molecular weight distribution, which in turn negatively affects the physical and chemical properties of the material (Eleni et al., 2011). Therefore, considerable research has been directed towards developing a prosthetic material that is chemically stable and environmentally resistant to ultraviolet radiation. The ideal material is yet to be realized (Eleni et al., 2011, Kiat-Amnuay et al., 2008, Fang et al., 2006, Polyzios et al., 2000).

As stated previously, color stability is the most significant challenge to maintaining the longevity of a maxillofacial prosthesis. Studies conducted during the past three decades have

evaluated the color stability of pigmented and non-pigmented maxillofacial silicon elastomers by adding inorganic opacifiers or organic ultraviolet radiation absorbers, and exposed materials to artificial and/or outdoor weathering (Kiat-Amnauy et al., 2006, Tran et al., 2004, Kiat-Amnauy et al., 2002). However, this approach is restricted by several factors, namely, the amount of additive that can be tolerated by the material without changing its baseline color and the fact that the solubility limit might be exceeded prior to reaching adequate ultraviolet radiation protection (Han et al., 2010). Another component of the color stability of a maxillofacial silicone elastomer is the stability of the pigment itself. Koran et al., studied the color stability of eleven maxillofacial pigments and found that all pigments demonstrated changes in at least one color parameter that was statistically significant (1979). Beatty et al., evaluated the color stability of five maxillofacial prosthetic pigments after 400 hour exposure to ultraviolet radiation and found that cadmium yellow medium and cosmetic red underwent substantial color change (1995). In their discussions they hypothesized that short-term color change may be attributed to color loss of non-UV-resistant pigments, whereas long-term color change may be attributed to the additional cross-linking and continued polymerization of the elastomer or by side reactions of impurities present within the silicone. Further compositional analysis would be required to confirm their hypothesis. A more recent study evaluated the color stability of oil pigments mixed with dry earth opacifiers after artificial weathering. They found that dry powder Ti white remained the most color stable over time. However, the authors reported that it possesses an intense color, making it difficult to use in the clinic as it tends to produce whiter samples (Kiat-Amnuay et al., 2006).

Two approaches have been taken to study the overall deterioration of maxillofacial materials. One approach is to expose materials to an accelerated weathering process. A common device is the weatherometer, an artificial weathering chamber first described by

Sweeny et al., in 1972. The second approach is to expose materials to outdoor weathering conditions and measure material property changes. Studies have shown that artificial weathering can be used to approximate the outdoor performance of maxillofacial elastomers as means to predict the overall lifetime of these polymers under service conditions. However, accelerated artificial weathering apparently influences the degradation mechanisms differently within the elastomer, and specific color changes often are not reproduced accurately (Gijsman et al., 1994, Sampers et al., 2002, Pospissil et al., 2006, Eleni et al., 2011).

Gary et al. (2001) measured color stability of pigmented and unpigmented silicon elastomers exposed to outdoor weathering in two different locations; Miami, FL and Phoenix, AZ based on their diverse climates. The mean color change was higher in Phoenix, AZ groups, indicating that an environment with low relative humidity and rainfall induces changes more rapidly compared to a moister environment, such as in Florida or Nebraska.

2.3 Nanoparticles.

2.3.1 Characteristics, Mechanical and Optical Properties

Nanoparticle-containing materials include those containing particles with approximate sizes of 5 to 100 nm, with shapes that can be spherical, cubic or needle-like (Cushing et al., 2004). As a particle is reduced in size from micrometer to nanometer, the resultant properties can change dramatically. For example, hardness, active surface area, chemical reactivity and biological reactivity are altered (Allaker & Ren 2008). The properties of nanoparticles can differ from those demonstrated by their bulk forms and in some cases give completely unexpected physical and chemical properties. For this reason industries in various fields (e.g. structural, biomedical, optical and electric) have extensively researched new processes that incorporate nanoparticles into polymeric matrices (Han et al., 2008). Carbon nanotubes have been studied

extensively. Studies have shown that carbon nanotubes, when incorporated into composite materials can produce high elastic modulus and increased strength, as compared to micro-fiber-reinforced composites (Thostenson et al., 2001). One study incorporated carbon nanotubes into elastomers and observed increased rigidity and shear modulus as compared to unfilled elastomers (Frogley et al., 2003). Nanoparticles are widely incorporated in industrial materials such as textiles, rubbers, sealants, plastics, cosmetics, fibers, coatings, sunscreens, dental composites and toothpastes. Nanoparticles are added to dental composites to improve the tooth-composite interface continuity and adhesive strength. Zinc citrate is incorporated into toothpastes to control plaque formation and titanium dioxide acts as a whitener (Tang et al., 2006). In elastomers, enhanced mechanical properties through nanoparticle additions may be attributed to a higher surface energy and chemical reactivity, which allow the nanoparticles to interact with the silicon backbone and form a three dimensional network (Watson et al., 2004).

Silicon dioxide (SiO_2), or silica, is used widely as a filler material in the micrometer size range to improve the mechanical properties of siloxane elastomers. Silica is most commonly found in nature as quartz and it is the major constituent of sand. It is mainly used in the construction industry to produce Portland cement, but other major applications include glass production, sand casting, and desiccants that are used in the food and pharmaceutical industries (Florke et al., 2008). Silica exists in many crystalline forms (polymorphic), but in most cases tetrahedral SiO_4^{4-} units are linked together with shared vertices in various arrangements. Silica nanoparticles have been used in paints to control rheological properties and also serve as reinforcing fillers in nanocomposites in order to improve tensile strength and wear and scratch resistance (Zheng at al., 2003).

Metal oxide nanoparticles impart the strength and mechanical properties desired from a

metal, and the decreased size imparts reduced opacity and improved overall optical properties. Metal-oxide nanoparticles, when incorporated into a polymer system, can show combined desired properties such as strength, hardness, elasticity, electrical conductivity and improved optical performance (Abdelsayed et al., 2006; Golden et al., 1995; Maiti et al., 2008. Khan et al., 2007). Khanna et al. (2007) have reported that rutile nano-TiO2 is used commonly as a white pigment due to its high light- scattering effect, which offers protection from ultraviolet radiation.

Rao et al., (2005) illustrated the use of nano-sized particles as a great advantage due to their large surface area. The surface area of particles for a given quantity of a material scales as 1/d where d is the average diameter of the particle. In the nanometric range, materials are expected to behave quite differently from both molecular and bulk states since the ratio of the number of surface atoms to the number of bulk atoms becomes significant (Rao et al., 2005, Mohseni et al., 2012). As a consequence of this increased ratio, the number of unsaturated valence atoms in the nanoparticles becomes significant, leading to higher chemical reactivity.

Several articles have been reported which studied composites filled with micro-sized particles. These studies indicated that microparticles improve physical properties and increase wear resistance in composite polymers due to their ability to form transfer films of the composites on the counterface, which are thin and uniform and are strongly bonded to the substrate. Composites filled with micro-sized copper compound fillers (CuO, CuS and CuF_2) loaded at 35 vol.% showed increased wear resistance compared to unfilled composites (Bahadur & Gong 1992). Sinha and Brisco (2009) examined strength and modulus of micro-filled composites and suggested that smaller filler particles contribute more to strengthening then do larger particles of the same compound.

When incorporating nanoparticle fillers into a polymer system, an essential criterion is the state of dispersion. The high chemical reactivity and specific surface area of nanoparticles results in very high attractive forces between the particles, thereby inducing a strong tendency to agglomerate (Wichmann et al., 2006). When nanoparticles agglomerate, they act as stress-concentrating centers, leading to a decrease in mechanical properties and a potential change in dimensional stability over time when a material is subjected to external forces (Han et al., 2008). However, if optimum dispersion is obtained, a homogeneously nanofilled polymer is produced, with improved resistance to environmental stress-induced cracking and aging (Liu et al., 2005).

A number of nano-sized metal oxides have been studied as polymer additives for gaining improvements in physical, mechanical and optical properties. Titanium dioxide is one, and it has found application as a pigment, adsorbent and catalyst (particularly photocatalyst) (Khanna et al., 2007). Titanium dioxide is polymorphic and exists in three forms; anatase, rutile and brookite (El Gorsey et al., 2001). The anatase crystalline phase exhibits the highest photocatalytic activity due to its large band gap energy of 3.2 eV and it is used in solar energy conversion because of its high photoactivity (Xu et al., 2002). Rutile-TiO_2 is called the “white pigment” and it provides protection from ultraviolet radiation due to its scattering effect (Khanna et al., 2007). Two theories have been suggested to explain the scattering effect of TiO_2. First, the Mie light scattering theory that predicts the optimum particle size of conventional TiO_2 to obtain maximum light scattering and opacity in the visible spectrum. This theory governs the scattering effect of larger TiO_2 particles and explains their optical properties. Second, Rayleigh’s light scattering theory implies that shorter wavelengths of light are more effectively scattered by smaller particles such as ultrafine TiO_2 nanoparticles. According to latter theory, the peak of scattering intensity is reached when the particle’s diameter is equal to one half the wavelength of UV light which means more forward scattering and less diffuse scattering. This explains the

UV blocking capabilities of TiO_2 nanoparticles (Allen et al., 2002, Yang et al., 2004). In addition to optical and UV blocking capabilities, TiO_2 nanoparticle additions have been shown to improve mechanical properties. One weight percent additions to resin based composite restorative materials increased microhardness by approximately 60% and flexural strength by 16% compared to unfilled composite (Xia et al., 2008). For color improvement, 0.1 to 0.25 weight percent additions better simulated the opalescence of human enamel (Yu et al. 2009).

Zirconia is a metal oxide ceramic known for superior mechanical properties, excellent optical properties and biocompatibility. Recently zirconia use has remarkably increased in dental restorative and prosthetic treatments (Denry & Kelly 2008; Thompson 2011). It is not soluble in water, is non-cytotoxic (Dion et al., 1994), does not enhance bacterial adhesion (Rimondini et al., 2002), is opaque and possesses low corrosion potential (Denry & Kelly 2008). Zirconia is polymorphic and allotropic, existing in three crystalline configurations at different temperatures: cubic, tetragonal and monoclinic (Lughi & Sergo 2010). During cooling the tetragonal phase transforms into a stable monoclinic phase. This is accompanied by a 4-5% crystal volume increase, which leads to internal compressive stress and potential cracking. In order to prevent the transformation and stabilize zirconia, it is often combined with other cubic oxides, notably MgO, CaO, Y_2O_3 and CeO_2 (Zarone et al., 2011). Zirconia, when used as a core material for single crowns and fixed partial dentures, enjoys a success rate of 93% over three years (Ortorp et al., 2009).

Silver ions and compounds have been extensively investigated for their antibacterial, antiviral and antifungal properties (Morones et al., 2005; Monteiro et al., 2009). In dentistry, silver has been used as an antimicrobial agent in dental composites (Herrera et al., 2001). Several studies have shown that Ag nanoparticles possess encouraging levels of antimicrobial

activity, as biocidal activity has been reported against gram positive, gram negative and pathogenic bacteria, in addition to normal flora (Li et al., 2005; Rai et al., 2009;Allaker 2010). Importantly, silver has rarely caused resistant microorganisms to develop (Dorjnamjin et al., 2008). Silver nanoparticles inhibit *C. albicans* growth at 0.2 μg/ml concentrations, which is less than that required to produce toxic effects against human fibroblasts (30 μg/ml) (Panacek et al., 2009). When silver nanoparticles were incorporated into experimental composite adhesives, rougher surfaces resulted, but they showed less bacterial adhesion and similar mechanical properties to conventional adhesives (Ahn et al., 2009).

2.3.2 Antifungal Effects of Nanoparticles

Nanoparticles have been used in controlling oral biofilm formation through different approaches, including biocidal, anti-adhesive and through delivery of antimicrobial agents and ligands (Allaker 2010). Nano-oxides, and particularly zirconia, have shown to be suitable carriers for antifungal agents, due to a high coordination number and the ability to form stable complexes (Malghe et al., 2009). The mechanism of action by which nanoparticles exert an antimicrobial effect is not fully understood. Certain studies suggest that nanoparticles prevent DNA replication by inactivating enzymes necessary for ATP production (Feng et al., 2000; Yamanaka, 2005). Others have suggested that electrostatic attraction between positively charged metal ions and negatively charged microbial cell membrane is critical for antimicrobial activity (Kim et al., 2007). It has been hypothesized that silver ions inactivate membrane-bound respiratory enzymes of microorganisms (Allaker 2010). Maxillofacial materials exhibiting the highest surface hydrophobicity also demonstrate the greatest antifungal effect (Nikawa et al., 1994). Nanoparticles have great potential use for this application, as they can increase hydrophobicity and surface charge in addition to chemical reactivity (Allaker 2010).

2.4 Gap in Knowledge

To date, most attempts to improve facial prosthesis longevity have focused on micro-sized additives, which have produced minimal improvements. More recent research has focused on nano-sized additives, which have shown success in improving mechanical and optical properties in the plastic, glass and paint industries, as well as emerging biomedical applications (Han et al., 2010). A gap in knowledge exists with regard to the extent nanoparticles may offer improvements in optical, physical and antifungal properties, in addition to prolonging prostheses lifetimes. Because titanium oxide provides excellent UV protection, zirconia offers enhanced mechanical properties and biocompatibility, and silver imparts antifungal activity, these three nanoparticles are the focus of this research. This study's purpose is to add different sizes of titanium oxide and zirconia nanoparticles to polydimethyl siloxane, and study color stability and selected physical properties following exposure to UVB radiation. A second purpose is to assess the antifungal activity of polydimethyl siloxanes containing TiO_2, ZrO_2 nanoparticles.

CHAPTER 3: MATERIALS AND METHODS

3.1 Preparation of Samples

Prototype pigmented elastomers were constructed by combining unpolymerized polydimethyl siloxane, nanoparticles, pigment, crosslinker and catalyst, and polymerizing the mixture under heat. Two sizes, with a ten-fold particle size difference, of TiO_2 and ZrO_2 nanoparticles were chosen for this project. Four experimental groups plus one material control group in addition to two Ag groups used as negative material control groups in antifungal experiments Table 3.1.

For elastomer preparation, 1% by weight of each experimental nanoparticle was mixed with 99 weight percent vinyl-terminated polydimethyl siloxane (PDMS) (V-2K, MW 23,000, polydispersity 2.5, Mat no. 057077, Momentive Materials, Tarrytown, NY). The nanoparticles were incorporated using a rotary mixer at 3000 rpm for five minutes. An ultrasonic mixer (Hielscher ultrasound processor model UP200S, Teltow, Germany) with a S3 Sonotrode at 100% amplitude (460 W/Cm^2) was used to burst nanoparticle agglomerates and disperse them into the vinyl-terminated PDMS. The ultrasonic mixer was housed in a sound box to minimize noise during mixing and the mixture was contained in a stainless steel malt cup that was cooled in an ice bath. Ultrasonic mixing proceeded for ten minutes, then each mixture was rotary mixed again with a Cowles disperser for ten minutes at 5000 rpm to achieve a uniform distribution of nanoparticles. Two weight percent functional intrinsic yellow pigment (FI-202, lot no. DL101606, Factor II, Inc., Lakeside, AZ) was added and rotary mixed at 5000 rpm for an additional five minutes. This yellow pigment was chosen because it was known to undergo substantial color change when subjected to environmental weathering (Gary and Smith, 1998, Kiat-amnuay et al., 2009).

Table 3.1. Nanoparticles Tested

Nanoparticle type	Size	Lot no.	Company
TiO_2	30-40 nm	54885-040108	Nanostructured and Amorphous Materials Inc. Houston, TX
TiO_2	200 nm	TI07193RUT11	Inframat Advanced Materials, Manchester, CT
ZrO_2	40 nm	USHT03	US Research Nanomaterials, Inc., Houston, TX
ZrO_2	200-300 nm	5970-061503	Nanostructured and Amorphous Materials Inc., Houston, TX
Ag	30-50 nm	USHW09	US Research Nanomaterials, Inc., Houston, TX
Ag	200-400 nm	0124-030413	Skyspring Nanomaterials, Inc., Houston, TX
SiO_4	200-300 nm	Unknown	Cabot Corporation, Boston, MA

Prior to initiating polymerization, each mixture was rotary mixed at 5000 rpm for 10 minutes to re-disperse the nanoparticles into the PDMS. For polymerization, equimolar ratios of the nanoparticle-containing vinyl-terminated PDMS were combined with polymethyl hydrogen siloxane (V-XL crosslinker, batch no. HVDD112906, Momentive Performance Materials, Friendly, WV) and 10 ppm platinum catalyst (VCAT-RT, lot no. 502L031798, OSi Specialties Inc., Sistersville, WV). The mixtures were mechanically spatulated in a paper cup for two minutes with a wooden tongue depressor, and air bubbles were removed under 5×10^{-3} torr constant vacuum by a high vacuum pump (Welch Vacuum Technology, Skokie, IL) attached to a bell chamber. Bubble removal was ascertained visually, and it typically required fifteen minutes. The mixtures were poured slowly into mold assemblies to allow the air from pouring to escape. A lid under load was placed on top of the molds to extrude excess material. The mold assemblies were placed into an 84 °C forced-air convention oven for sixty minutes for polymerization. Preliminary trials determined that mold assemblies containing large nanoparticles (200-400 nm) required the molds to be inverted every ten minutes to prevent nanoparticles from settling on one side of the elastomer. For the control group, 13% loading weight of fumed silica (to follow what is used currently in maxillofacial prosthetics) was added to vinyl-terminated polydimethyl- siloxane (PDMS) under 2000 rpm rotary mixer until fully dissolved, followed by 15-20 minutes of rotary mixing at 7000 rpms to ensure particle dispersion.

Test samples with different geometries were used for color, mechanical and antifungal activity measurements. Disk-shaped molds were used to fabricate samples for color change measurements and Durometer (Shore A) hardness. Mold assemblies consisted of polyvinyl chloride (PVC) pipes cut into 6 mm thick sections and secured with medium-body polyvinyl siloxane (PVS) impression material to a gypsum slab to mimic what is used in dental labs fabricating maxillofacial prosthesis. The mixture was poured slowly from one side into the mold

and a glass slab was placed to extrude any excess material. Four-inch vice clamps were used to secure the glass slab with approximately 2-5 kg of load. The resultant polymerized discs had a diameter of 38 mm and a thickness of 6 mm. Five discs per group were made, as previous studies showed significant difference color changes could be detected at an alpha level of 0.01 with power of 0.8 (Beatty et al., 1995).

For tensile properties, elastomer mixtures were poured onto gypsum molds and covered with a clear polycarbonate sheet (13'' × 10'' × 0.5'', USP Plastic Corporation, Lima, OH). The polycarbonate was secured with four-inch vice clamps, tightened to deliver approximately 2-5 kg of load in order to extrude excess materials. The resultant elastomer sheets were 254 mm length x 165 mm width x 2 mm thickness. Dumbbell-shaped samples were cut from these elastomer sheets using a die cutter that conformed to die C for ASTM Standard D412-08 (ASTM International Standards Worldwide, http://www.astm.org/Standards/D412.htm). For each experimental and control group, twelve dumbbells were constructed. A Nikon measurescope (MM-11) with computer software (Quadra-check 200) were used to measure width and depth of each sample at the dumbbell gage length. This information was used to calculate cross-sectional area, which was necessary for computing stress during generation of stress-strain curves.

3.2 Exposure to Ultraviolet Weathering

Each dumbbell or disc was placed on a reflective surface inside a plywood enclosure beneath four 36-inch bulbs (UVB Broadband Lamp, FS40T12, National Biological Corp., Twinsburg, OH) delivering UVB radiation with wavelength range from 290-315 nm. The enclosure was housed in an environmental chamber with controlled temperature and humidity throughout the experiment. Samples were placed 12 inches directly below the bulbs, and the surrounding environment was maintained at 25 °C and 30% relative humidity. Under these

conditions, radiation was delivered at 0.2 mW/cm^2 which was equivalent to 720 mJ/cm^2/hour, and the sample surface temperature did not exceed 0.5 °C above the surrounding environment, as measured by a thermocouple. According to Beatty et al., this UVB output reflected the average daily exposure from natural sunlight in Lincoln, NE during summer measured with UVB detector at noon. (1995) Light output was monitored continuously throughout the experiment using a light sensor and a data logger (UVB sensor, PMA 2100 logger, Solar Light Co., Philadelphia, PA).

In addition to ultraviolet radiation exposure, materials containing each nanoparticle type were stored in a weathering control environment (darkness, 25 °C, 30% relative humidity). This provided an assessment of potential material changes occurring over time without a weathering stimulus. Measurement times for color change and Shore-A hardness were chosen to permit comparison with previous research, which was set at 600, 1800 and 3000 hours. For mechanical testing, an extra set of test samples was constructed to establish baseline values, since the tensile tests were destructive in nature. For this same reason, mechanical tests could not be conducted at intermediate time intervals, making it necessary to obtain mechanical property values only at baseline and 3000 hours.

3.3 Color Measurements

Color measurements were made using a color reflectance spectrophotometer (CM-2002, Konica Minolta Corp., Ramsey, NJ) with computer software (SpectraMagic NX, Konica Minolta Corp., Ramsey, NJ). Color measurements were made on each disc at 0, 600, 1800 and 3000 hours according to the CIE L*A*B* system (Commission Internationale de l'Eclairge, 2004). The spectrophotometer determined color according to ASTM D2244-07 (2007, "Standard Practice for Calculation of Color Tolerances and Color Differences from Instrumentally Measured Color

Coordinates", ASTM international, West Conshohocken, PA, DOI: 10.1520/D2244-07). Three axes defined the color space; L* was the white-black axis, a* was the red-green axis and b* was the yellow-blue axis. At the beginning of each session the spectrophotometer was calibrated with black and white backgrounds. Black calibration was conducted with background lights turned off and white calibration was achieved with a white calibration plate. All measurements were made with samples resting on a standard white background plate (no. 21633347, Konica Minolta Corp., Ramsey, NJ) using 50 g weight with background lights turned on. Each disc was labeled with a code using permanent ink scribed on the side (along the thickness dimension). Color measurements were made on the disc face above the top of the scribed code. The spectrophotometer was placed with the measuring port facing upward and three tongue plates were placed underneath the body in a manner that the device was parallel with the floor. Each disc was oriented with the code placed in the same position at each time interval so that color measurements would be taken at the same location. Once color measurements were completed, UVB samples were immediately returned to the weathering chamber and control samples placed in the control environment.

After recording L*, a* and b* values in an Excel spreadsheet, color differences (ΔL*, Δa* and Δb*) were calculated for each sample at each time interval. Total color change (ΔE*) was calculated from the equation $\Delta E^* = [(\Delta L^*)^2+(\Delta a^*)^2+(\Delta b^*)^2]^{1/2}$.

3.4 Physical Properties Measurements

3.4.1 Tensile Property Measurements

For tensile testing a universal testing machine (Instron 1123-5500R, Instron Corp., Boston, MA) and computer software (M-Bluehill-K2-EN Revision A) were used to perform the tests and record data. Dumbbell-shaped samples (n=12 per group) were measured for thickness

and width, loaded into grips, and a long-travel extensometer with a 25 mm gauge length was attached. Each dumbbell was elongated at a rate of 500 mm/min and stress versus strain data were graphically charted and digitally recorded until failure. Three properties were determined, ultimate tensile strength, total strain at failure and modulus of elasticity. Ultimate tensile strength was considered to be the maximum stress the test sample could withstand, which usually occurred at failure. Maximum strain at break was a measure of the total amount of extension a material could withstand prior to failure. The maximum tensile displacement of a sample was divided by the starting length to obtain maximum strain at break and was expressed as mm/mm. Modulus of elasticity was calculated as the slope of a linear portion of the stress-strain curve between 50% and 100% strain. Tensile testing was performed at baseline and after 3000 hours of exposure to both control and UVB environments.

3.4.2 Shore A Hardness

For Durometer hardness tests, the same discs as for color measurements were used (n=5 per group). A shore A hardness tester (Instron Durometer Type A, Model DRCL, ASTM D2240, Instrument & Manufacturing Company Inc., Freepost, NJ) was used to measure hardness at baseline (zero), 600, 1800 and 3000 hours of storage in control or UVB environments. Hardness measurements were taken on the opposite face from that used to obtain color measurements. This procedure was followed because the Durometer indenter had the potential to deform the elastomer and affect color measurements, which were taken at the same session. Hardness measurements were made following ASTM D2240 protocol; five measurements were made at random locations and the average of these readings was considered to be the representative hardness value.

3.5 Antifungal Activity

3.5.1 *Candida albicans* and Growth Conditions

C. albicans wild-type strain(CA42), formerly known as SC5314), was grown aerobically in yeast nitrogen base (YNB) medium (Difco Laboratories, Detroit, MI) on fresh Sabouraud Dextrose Agar plate (Difco Laboratories, Detroit, MI). The plate was incubated for 24 hours at 37℃ on a shaker at 60 rpm (model classic C25, New Brunswick Scientific, Edison, NJ). Cells were harvested and washed three times with 0.15 M phosphate-buffered saline (Gibco PBS; pH 7.4, Ca^{+2} and Mg^{+2} free, Life technologies, Grand Island, NY). Cells were resuspended in 10 ml PBS, counted with a hematocytometer and used within 24 hours.

3.5.2 Biofilm Formation

Test samples consisted of circular disks stamped from the remnants of silicon elastomer sheets that were used to make dumbbell-shaped samples for tensile tests. A circular punch (9-Piece Hollow Punch Set, SKU No. P3838, Central Forge, Pittsburg, PA) was used to create these disks with 2mm thickness and 12.7 mm diameter. Twelve disks per group were created for the four experimental groups (TiO_2, ZrO_2), positive material control group (silica), and two negative material control groups (Ag). Silver nanoparticles were added to PDMS at a concentration of 1 μg/ml. This concentration was chosen due to its potential antifungal activity while remaining at a concentration below potential toxicity (30 μg/ml) (Panacek et al., 2009). Disks were sterilized in an autoclave at 120℃ and 16 psi for 30 minutes.

The biofilm formation protocol used in this study followed that described by Kuhn et al., 2002. All discs were preconditioned with fetal bovine serum (Gibco FBS; Life technologies, Grand Island, NY) in a 96-well tissue culture plate (Falcon Microtest Tissue culture Plate, 96 well, Flat Bottom with Low Evaporation Lid, Becton Dickinson Labware, Franklin Lakes, NJ) and incubated

at 37℃ for 24 hours. FBS was removed and gently washed with 0.15 M PBS to remove residual FBS. 200 μL of fresh YNB medium was added to each well, followed by 200 μL of *C. albicans* cell suspension in a concentration of 1×10^8 cells/ml, which yielded 20,000 cells per well. The plate was incubated for 90 minutes in 5% CO_2 at 37℃ on a rocker table at 60 rpm to develop the adhesion phase of the *C. albicans* biofilm. Samples were washed with PBS to remove unattached cells, covered with 200 μL of YNB and incubated for 48 hours in 5% CO_2 at 37℃ on a rocker table at 60 rpm to provide a suitable environment for the biofilm maturation phase.

In addition to positive and negative material control groups, which consisted of silica and silver nanoparticles, a positive biological control group was included which entailed constructing wells containing YNB and *C. albicans*. Two methods were performed to measure antifungal activity: XTT colorimetric assay and confocal laser scanning microscopy (CLSM).

3.5.3 XTT Colorimetric Assay

C. albicans biofilm formation on test samples was quantified using a tetrazolium salt-based 2,3-bis (2-methoxy-4-nitro-5-sulfophenyl)-5-([phenyl amino] carbonyl)-2H-tetrazolium hydroxide (XTT) colorimetric assay, as described by Chandra et al. (2008). This method measures enzyme activity that reduces XTT dye to water-soluble formazan dye. The XTT assay is rapid, reproducible, non-invasive, non-destructive and requires minimal post-processing of samples (Ramage et al., 2009). The reduction of XTT to formazan crystals can only take place in the presence of viable cells and the necessary reductase enzymes. Therefore, the XTT assay measures the optical density of formazan crystals in solution as an indication of the metabolic activity of viable *C. albicans* cells. Immediately after biofilm maturation, YNB was removed, test samples were washed with PBS and samples were transferred to a new 96-well tissue culture plate. 200 μl PBS, 50 μl XTT (1 mg/ml in PBS) and 4 μl menodine solution (1 mmol/L in acetone)

were added to each well in the new 96-well plate for test groups, and to the old 96-well plate for control groups. Plates were incubated in darkness at 37℃ for 5 hours. The suspension was then measured spectrophotometrically (Elx808 Absorbance Microplate Reader, BioTek, Winooski, VT) at 492 nm. At this wavelength the absorbance of the water-soluble orange formazan dye end-product can be measured.

3.5.4 Confocal Laser Scanning Microscopy (CLSM)

Biofilm formation was also evaluated qualitatively using confocal laser scanning microscopy. The protocol used was described previously by Chandra et al. (2008). Two samples of each group were transferred carefully to preserve biofilms to a 12-well culture plate and incubated for 45 minutes at 37 ℃ in 2 ml PBS containing the fluorescent stain FUN-1 (lot # 745237, excitation wavelength= 488 nm and emission wavelength= 505 nm, Invitrogen, Molecular Probes, Eugene, OR) that emits green fluorescence when diffused into cytoplasm, and is converted over time by metabolically active enzymes into orange-red cylindrical intravascular structures. After incubation, silicon elastomer discs were turned over and placed on a 35 mm diameter glass-bottom petri dish (MatTech corp., Ashland, MA). An Olympus FV500 system on an IX81 scope (inverted microscope) was used with 40× lens, located in the microscopy core facility at UNL center for biotechnology (Dr. You Zhou, University of Nebraska-Lincoln). Multiple photomicrographs (using 488 nm excitation laser line and 505 nm emission filter) were taken from different areas of each sample to evaluate the architecture of *C. albicans* biofilm growth on elastomer discs.

3.6 Data Analysis

For color data analyses, group means and standard errors were calculated for dependent variables ΔL*, Δa*, Δb* and ΔE*. Independent variables influencing color were weathering environment (control and UVB), filler content (13% silica, 1% TiO_2 200 nm, 1% TiO_2 30-40 nm, 1% ZrO_2 200 nm and 1% ZrO_2 40 nm) and time (600, 1800 and 3000 hours). The null hypothesis that color change was not affected by nanoparticle addition, weathering exposure and time was tested by a three-way analysis of variance (ANOVA), followed by a Tukey-Kramer *post hoc* test for pairwise comparisons at a ($p<0.05$) level of confidence.

For changes in Shore A hardness, means and standard errors were calculated as dependent variables. Independent variables influencing hardness were the same as those described for color. The null hypothesis that Shore A hardness change was not affected by nanoparticle addition, weathering exposure and time was tested by a three-way analysis of variance (ANOVA) followed by a Tukey-Kramer *post hoc* test for pairwise comparisons at a ($p<0.05$) level of confidence. For tensile properties, group means and standard errors for ultimate tensile strength, strain at break and modulus of elasticity were calculated as dependent variables. Independent variables were test condition (immediate (baseline), 3000 hours control and 3000 hours UVB) and filler content (13% silica, 1% TiO_2 200 nm, 1% TiO_2 30-40 nm, 1% ZrO_2 200 nm and 1% ZrO_2 40 nm). A two-way analysis of variance (ANOVA) followed by a Tukey-Kramer *post hoc* test for pairwise comparisons at a ($p<0.05$) confidence level was used to test the null hypothesis that tensile properties of PDMS elastomers were not affected by nanoparticle addition.

For antifungal activity, a linear least square model was constructed, followed by a Dunnett adjustment to compare group means and standard errors of XTT absorbance to the

positive control group at a ($p<0.01$) confidence level. The null hypothesis tested was that nanoparticle addition did not affect antifungal activity of PDMS elastomer.

CHAPTER 4: RESULTS

4.1 Color Measurements

Baseline color measurements (L*, a* and b*) for each group are presented in Fig 4.1 and Table 4.1. From these data ΔL*, Δa*, Δb* and ΔE* were calculated for each time interval (600 h, 1800 h and 3000 h) of exposure to control or UVB weathering conditions.

A three-way ANOVA determined that significant differences were present among nanoparticle type, weathering condition and time of exposure for each color parameter. Therefore, ANOVA was followed by a Tukey-Kramer *post hoc* test to compare differences and determine which interaction was significant.

Table 4.1. Baseline Color Parameters Values (Mean (S.D.), n=10)

Group	L*	a*	b*
TiO_2 200 nm	90.31 (0.39)	-0.62 (0.25)	55.60 (0.32)
TiO_2 30-40 nm	88.73 (0.18)	0.85 (0.07)	60.06 (0.66)
ZrO_2 200 nm	79.17 (0.41)	4.41 (0.14)	88.76 (1.87)
ZrO_2 40 nm	79.75 (0.31)	4.13 (0.12)	91.48 (0.87)
Silica 200-300 nm	79.52 (0.27)	4.27 (0.07)	93.18 (1.41)

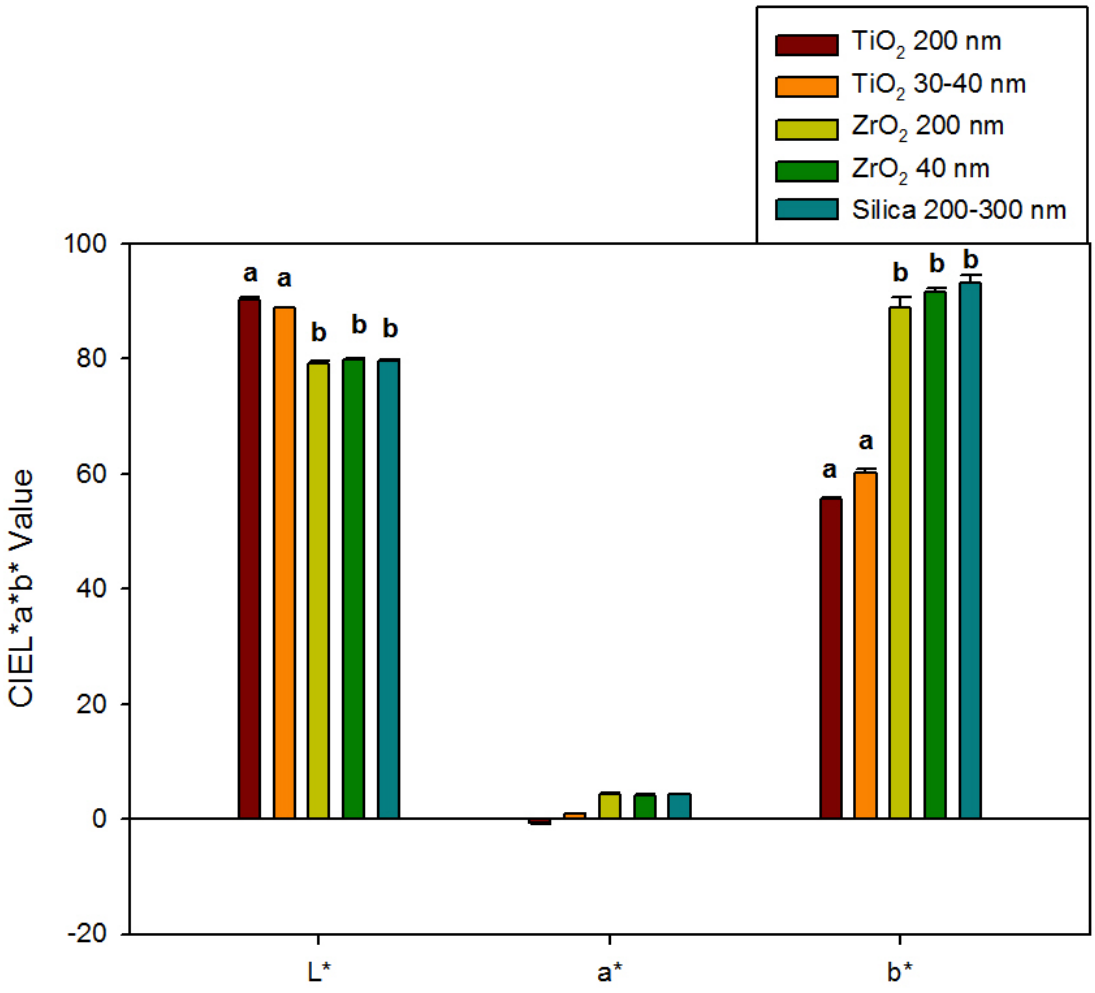

Figure 4.1. Bar graph displaying means and standard deviations (error bars) of baseline color parameters L*, a* and b* for different groups (n=10). Means with the same lowercase letters are not significantly different ($p \geq 0.05$). No statistical difference detected in a* of any materials.

4.1.1 After 600 Hours of Weathering

In the control groups, ΔL* value (which represent, the white-black axis in the CIE L*a*b* color system) for 40 nm ZrO_2 group was statistically significantly lower (darker) than 30-40 nm TiO_2 and silica groups ($p<0.05$, Fig 4.2). Under UVB weathering, 200 nm TiO_2 was significantly less negative (whiter) compared to all other groups ($p<0.05$, Fig 4.2). Also, the 30-40 nm TiO_2 group was whiter than both ZrO_2 groups and the silica group ($p<0.05$, Fig 4.2).

For red- green color change, negative Δa* values denoted increased greening after 600 hours of control weathering. The 30-40 nm TiO_2 group was less green when compared to other nanoparticle groups ($p<0.05$, Fig 4.3) but not significantly different when compared to the silica group ($p\geq0.05$, Fig 4.3). For UVB weathering, positive Δa* values indicated less green was present, with 200 nm TiO_2 materials being significantly greener compared to the other groups ($p<0.05$, Fig 4.3). 30-40 nm TiO_2 Δa* values were lower than both ZrO_2 groups, and silica was higher (less green) than all other groups ($p<0.05$, Fig 4.3).

For Δb* (yellow-blue), values measured in the control weathering environment were lowest (least yellow) for the 200 nm ZrO_2 group ($p<0.05$, Fig 4.4) with no statistically significant differences noted between the other groups ($p\geq0.05$, Fig 4.4). After 600 hours of UVB exposure, both TiO_2 groups were less negative (more yellow) compared to the other three groups ($p<0.05$, Fig 4.4).

Table 4.2. ΔL*, Δa*, Δb* and ΔE* values after 600 hours of weathering (Mean (S.D.), n=5)

Color Parameter/ Weathering	TiO_2 200 nm	TiO_2 30-40 nm	ZrO_2 200 nm	ZrO_2 40 nm	Silica 200-300 nm
ΔL*					
Control	-0.71 (0.07)	-0.31 (0.03)	-0.72 (0.16)	-0.88 (0.07)	-0.32 (0.06)
UVB	-1.48 (0.08)	-2.05 (0.09)	-4.48 (0.19)	-4.31 (0.13)	-4.37 (0.12)
Δa*					
Control	-0.53 (0.02)	-0.25 (0.02)	-0.68 (0.02)	-0.67 (0.03)	-0.32 (0.02)
UVB	0.28 (0.02)	0.51 (0.03)	0.95 (0.06)	0.90 (0.10)	1.78 (0.06)
Δb*					
Control	-1.24 (0.12)	-0.46 (0.20)	-2.62 (0.45)	-1.56 (0.12)	-0.39 (0.43)
UVB	-2.15 (0.12)	-3.32 (0.11)	-7.04 (0.34)	-7.00 (0.09)	-6.91 (0.23)
ΔE*					
Control	1.53 (0.12)	0.71 (0.08)	2.85 (0.40)	1.91 (0.12)	1.02 (0.15)
UVB	2.63 (0.13)	3.94 (0.15)	8.40 (0.37)	8.27 (0.14)	8.37 (0.24)

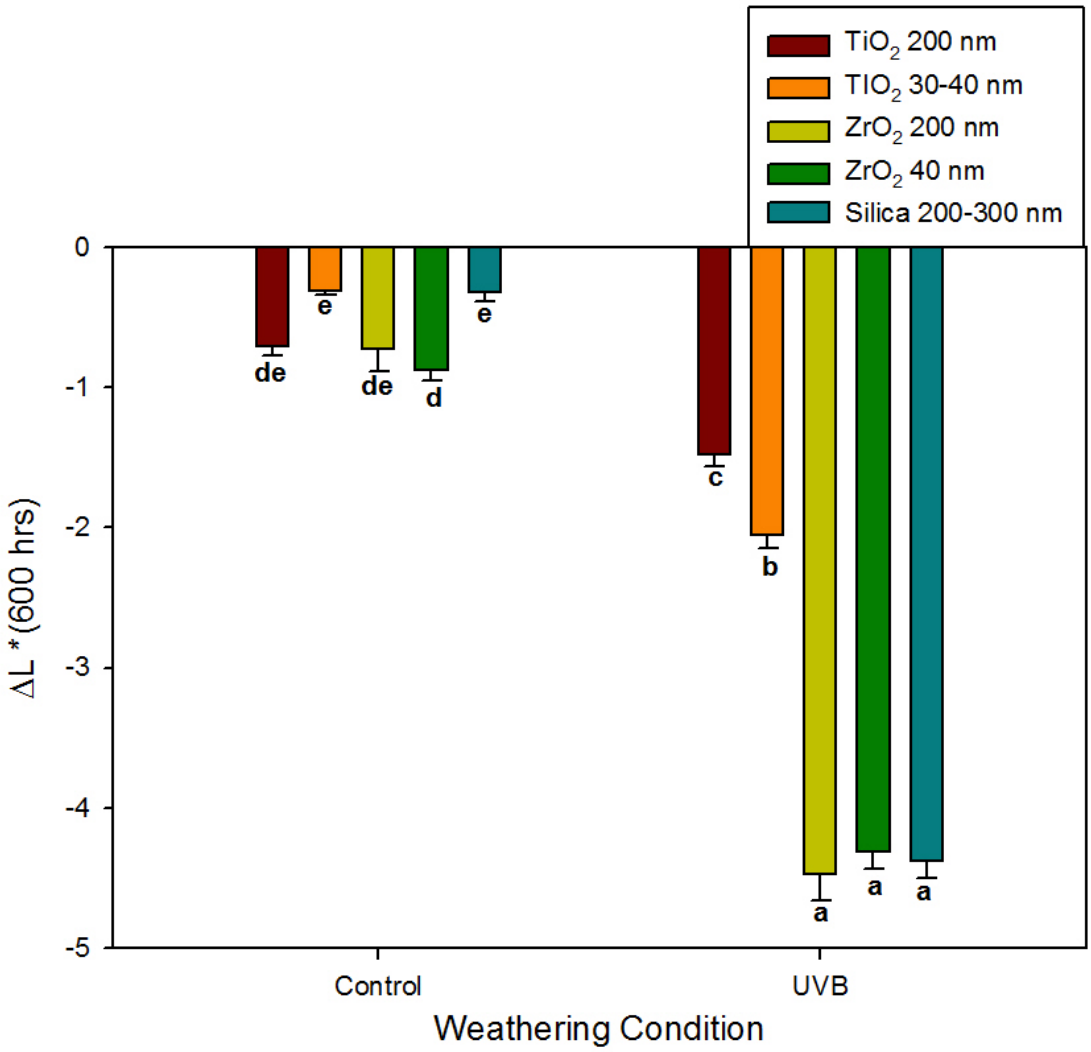

Figure 4.2. Bar graph displaying means and standard deviations (error bars) of ΔL* after 600 hours weathering for different groups (n=5). Means with the same lowercase letters are not significantly different ($p \geq 0.05$).

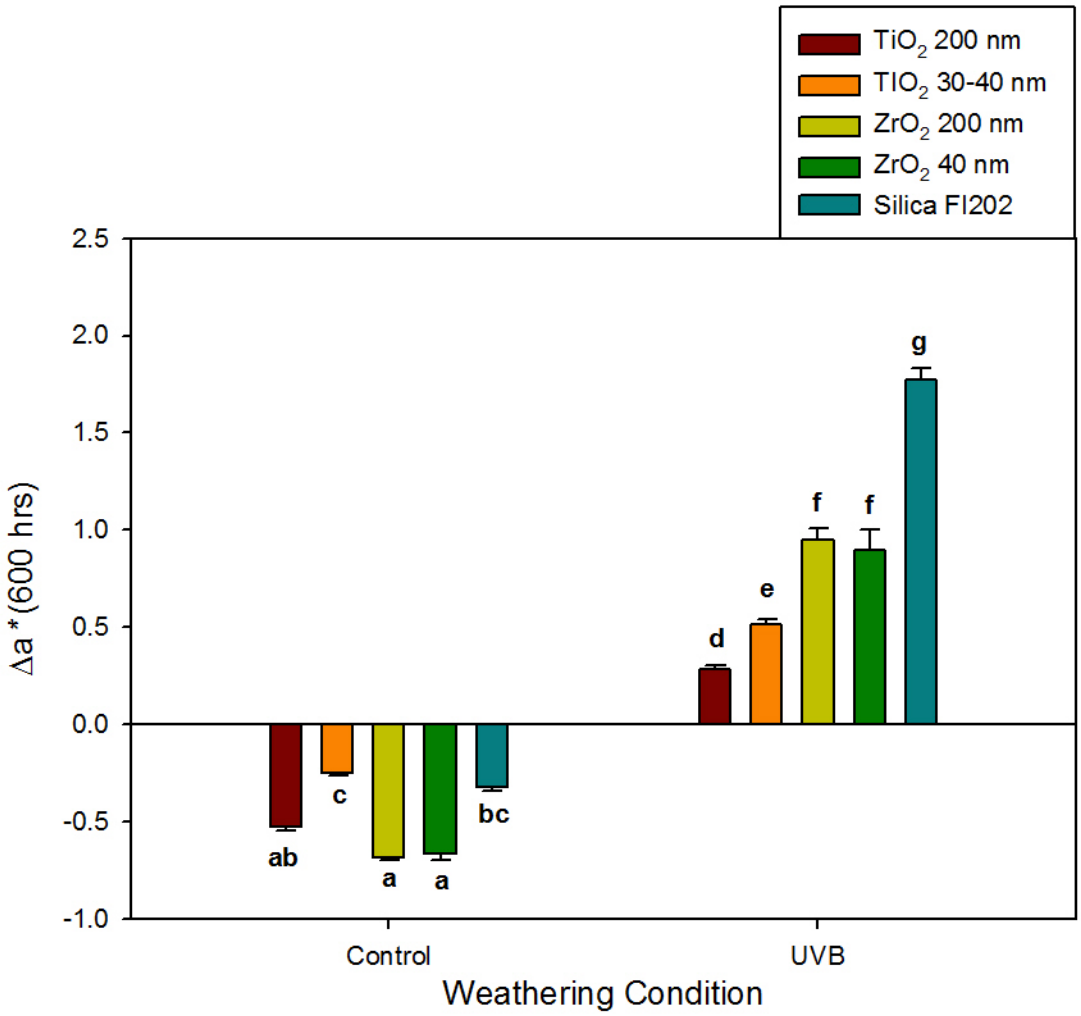

Figure 4.3. Bar graph displaying means and standard deviations (error bars) of Δa* after 600 hours weathering for different groups (n=5). Means with the same lowercase letters are not significantly different ($p \geq 0.05$).

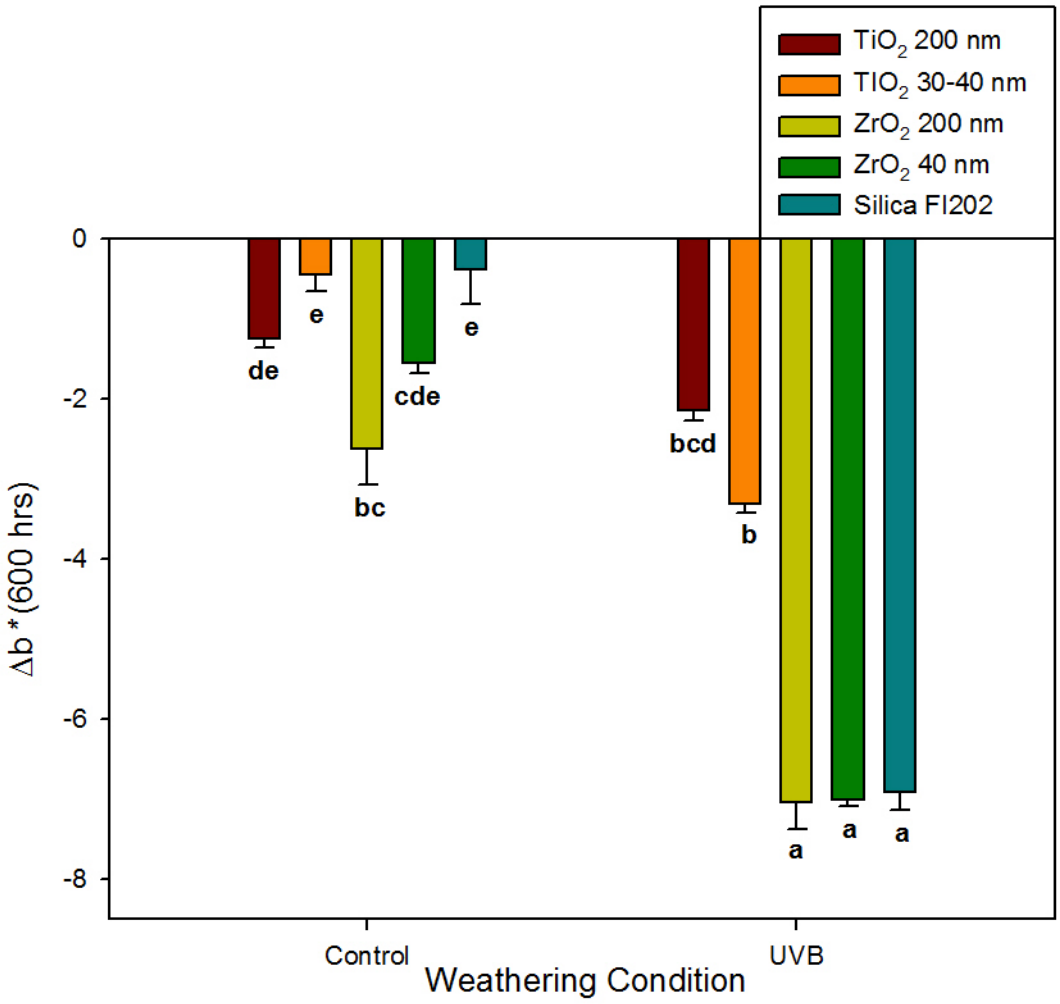

Figure 4.4. Bar graph displaying means and standard deviations (error bars) of Δb* after 600 hours weathering for different groups (n=5). Means with the same lowercase letters are not significantly different ($p \geq 0.05$).

Overall color change ΔE* was lowest for the 30-40 nm TiO_2 and silica groups in the control weathering environment ($p<0.05$, Fig 4.5). Both were below the perceptible color change threshold of 1.1, while all groups were below the acceptable color change threshold of 3.0. In terms of UVB weathering, 200 nm TiO_2 demonstrated the lowest color change, followed by 30-40 TiO_2 group ($p<0.05$, Fig 4.5). All groups were well above the acceptable color change threshold except for 200 nm TiO_2, with a ΔE* of 2.63.

4.1.2 After 1800 Hours of Weathering

For the 30-40 nm TiO_2 and silica groups, ΔL* and Δa* values were significantly less negative (whiter and less green) than the other three groups when stored in control conditions ($p<0.05$, Fig 4.6 and 4.7). In UVB weathering, ΔL* and Δa* values for 200 nm TiO_2 was highest, then followed by the 30-40 nm TiO_2 group ($p<0.05$, Fig 4.6 and 4.7). The silica group showed the highest positive change in the Δa* parameter (more green, $p<0.05$, Fig 4.7).

Δb* values after 1800 hours of control weathering showed that the 200 nm ZrO_2 group was more negative (less yellow) when compared to the two TiO_2 groups and the silica group ($p<0.05$, Fig 4.8). The 30-40 nm TiO_2 group was less negative (more yellow) compared to the ZrO_2 groups ($p<0.05$, Fig 4.8). In UVB weathering, Δb* values for 200 nm TiO_2 were the least negative, followed by the 30-40 nm TiO_2 group ($p<0.05$, Fig 4.8).

With respect to overall color change under control conditions, ΔE* values for 30-40 nm TiO_2 in control weathering were significantly lower than all other groups, but overlapped with the silica group ($p<0.05$, Fig 4.9). 200 nm ZrO_2 underwent the highest color change, which was significantly greater than the other groups except 40 nm ZrO_2 ($p<0.05$, Fig 4.9). The 30-40 nm TiO_2 was the only group below the perceptible color change threshold, while 200 nm ZrO_2 was the only group above the acceptable color change threshold. With regard to UVB weathering

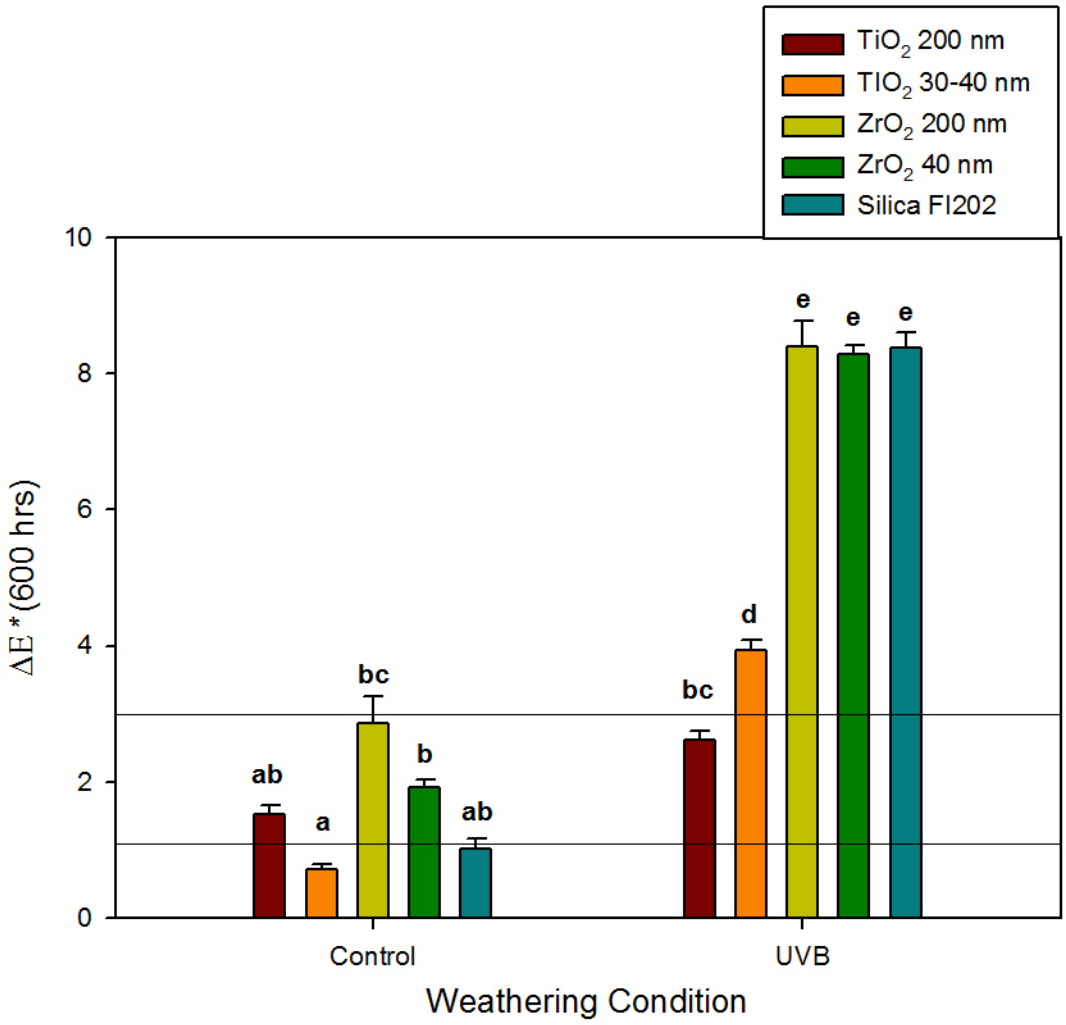

Figure 4.5. Bar graph displaying means and standard deviations (error bars) of ΔE* after 600 hours weathering for different groups (n=5). Means with the same lowercase letters are not significantly different ($p \geq 0.05$). Lines drawn at ΔE* = 1.1 and 3.0 represent the minimum thresholds for 50:50 visual perceptibility and acceptability, respectively.

Table 4.3. ΔL*, Δa*, Δb* and ΔE* values after 1800 hours of weathering (Mean (S.D.), n=5)

Color Parameter	TiO_2 200 nm	TiO_2 30-40 nm	ZrO_2 200 nm	ZrO_2 40 nm	Silica 200-300 nm
ΔL*					
Control	-1.00 (0.09)	-0.42 (0.05)	-1.41 (0.04)	-1.19 (0.08)	-0.60 (0.09)
UVB	-2.71 (0.02)	-3.64 (0.07)	-6.99 (0.10)	-6.14 (0.11)	-7.36 (0.08)
Δa*					
Control	-0.55 (0.04)	-0.22 (0.02)	-0.83 (0.02)	-0.74 (0.03)	-0.31 (0.02)
UVB	1.22 (0.04)	1.49 (0.02)	1.79 (0.05)	1.73 (0.07)	3.05 (0.04)
Δb*					
Control	-1.65 (0.13)	-0.60 (0.29)	-3.09 (0.29)	-2.43 (0.21)	-1.30 (0.42)
UVB	-4.19 (0.09)	-6.00 (0.09)	-11.57 (0.26)	-10.57 (0.34)	-12.31 (0.12)
ΔE*					
Control	2.01 (0.16)	0.89 (0.20)	3.50 (0.27)	2.82 (0.21)	1.58 (0.31)
UVB	5.14 (0.07)	7.18 (0.11)	13.64 (0.26)	12.35 (0.33)	14.67 (0.08)

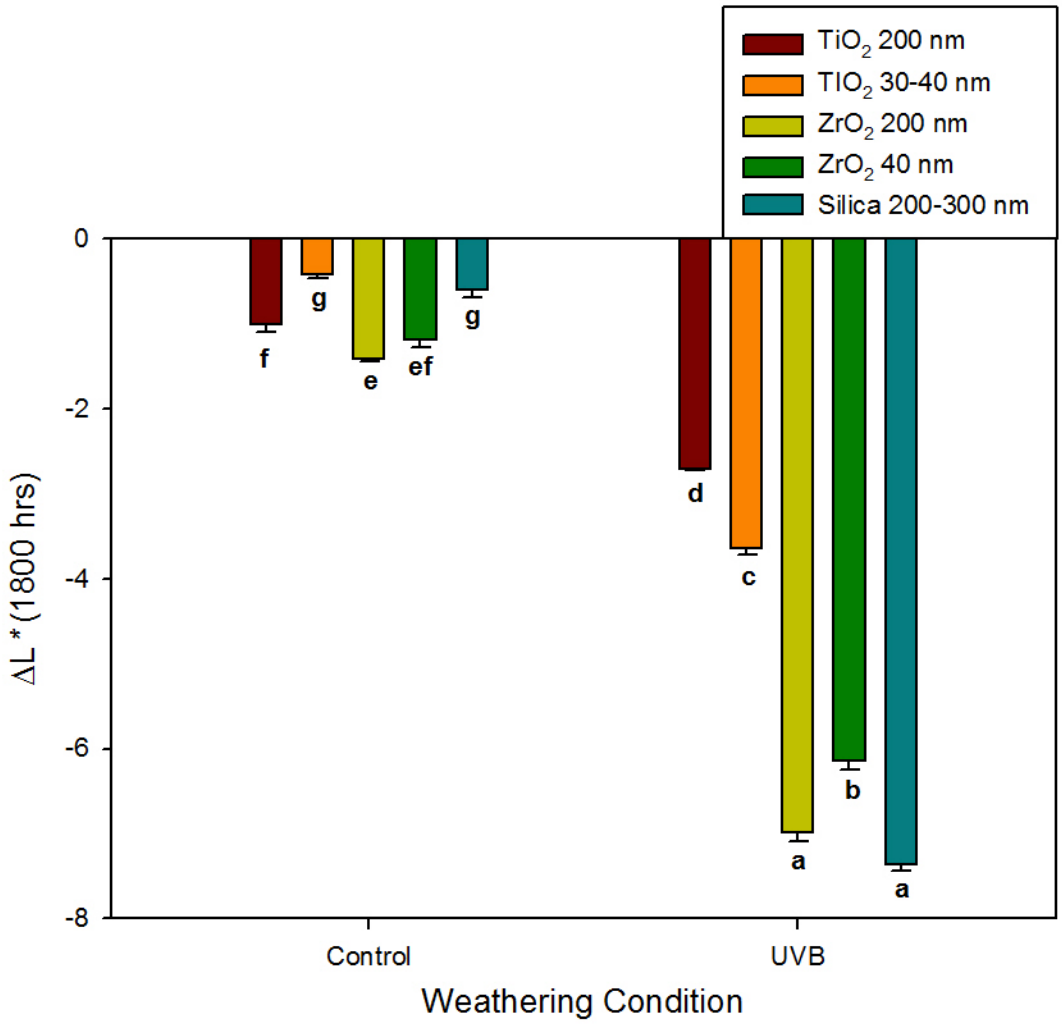

Figure 4.6. Bar graph displaying means and standard deviations (error bars) of ΔL* after 1800 hours weathering for different groups (n=5). Means with the same lowercase letters are not significantly different ($p \geq 0.05$).

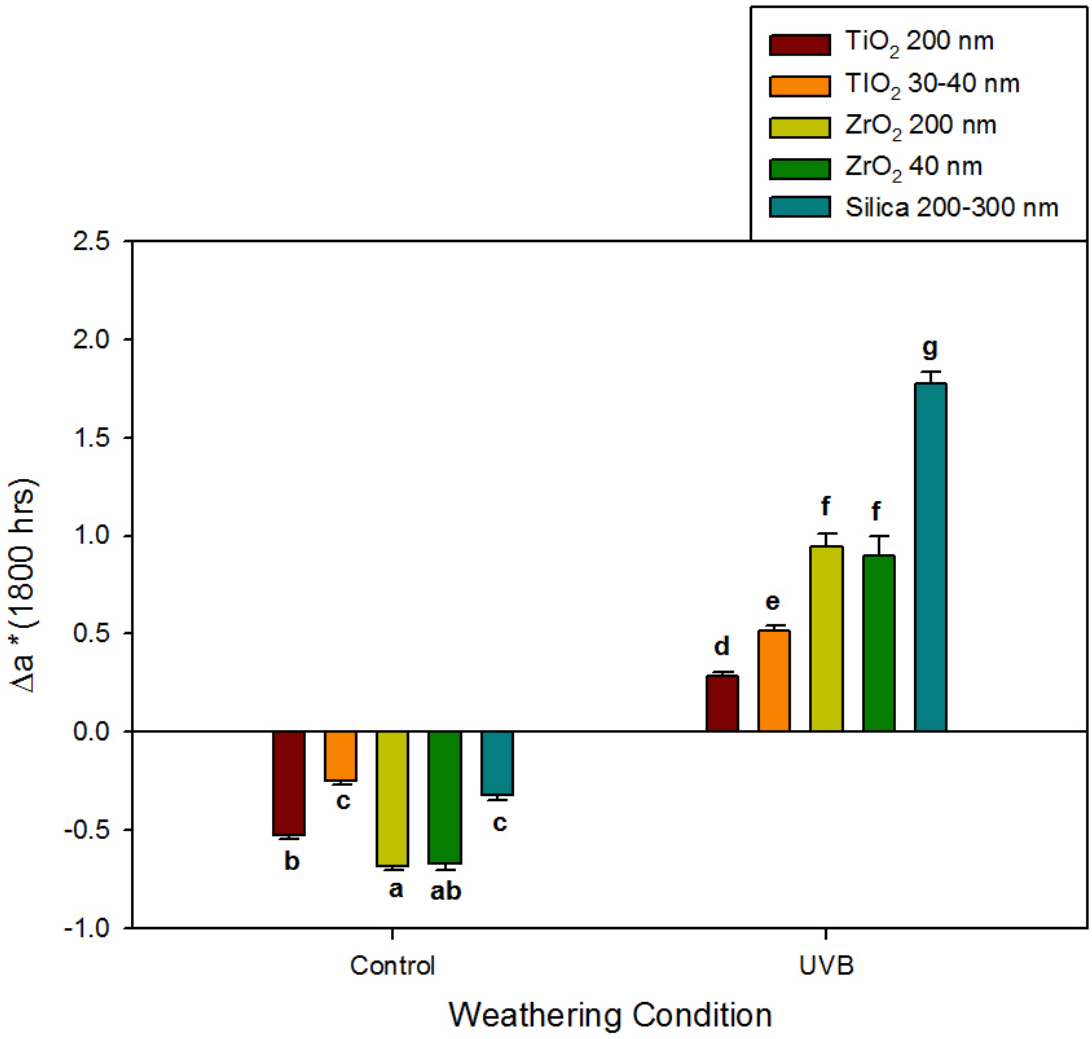

Figure 4.7. Bar graph displaying means and standard deviations (error bars) of Δa* after 1800 hours weathering for different groups (n=5). Means with the same lowercase letters are not significantly different ($p \geq 0.05$).

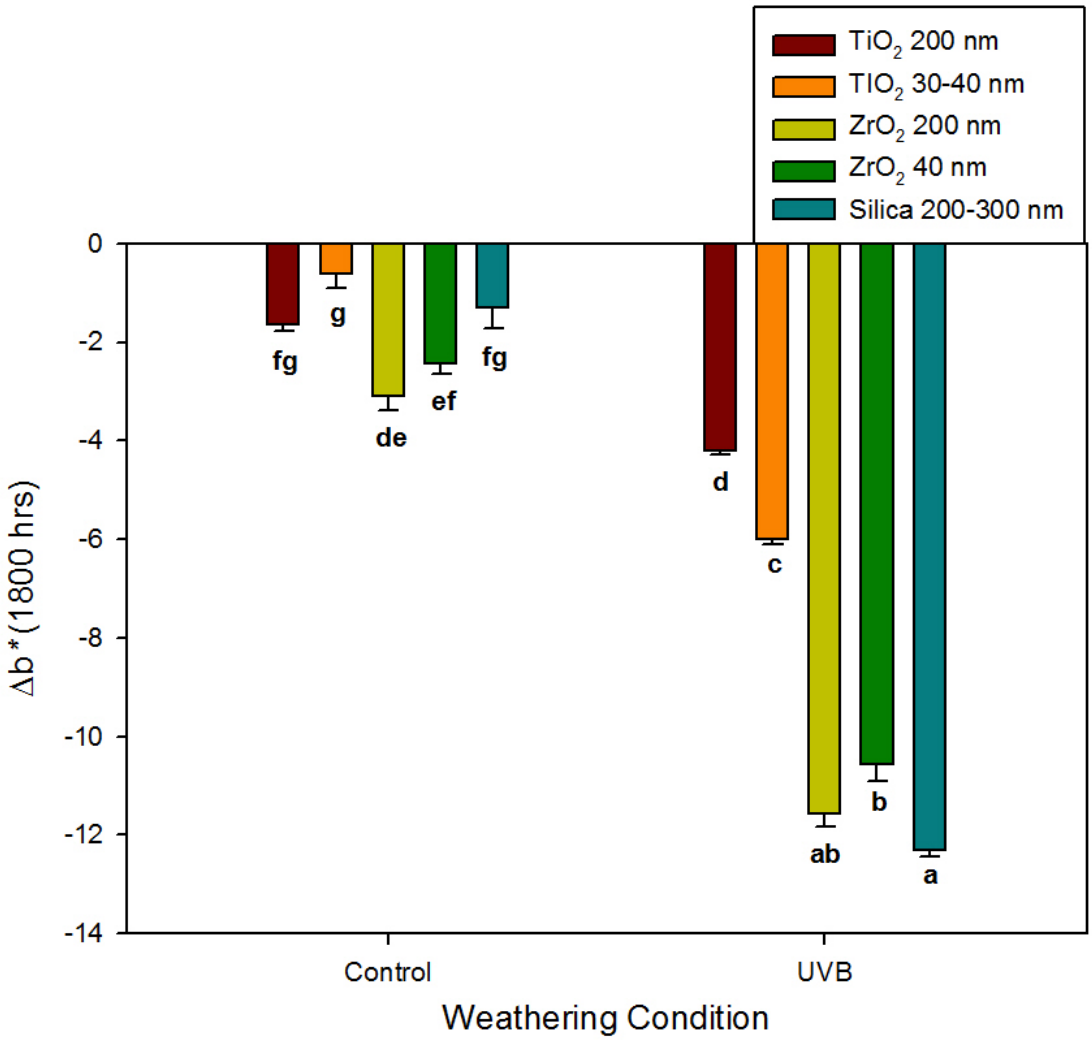

Figure 4.8. Bar graph displaying means and standard deviations (error bars) of Δb* after 1800 hours weathering for different groups (n=5). Means with the same lowercase letters are not significantly different ($p \geq 0.05$).

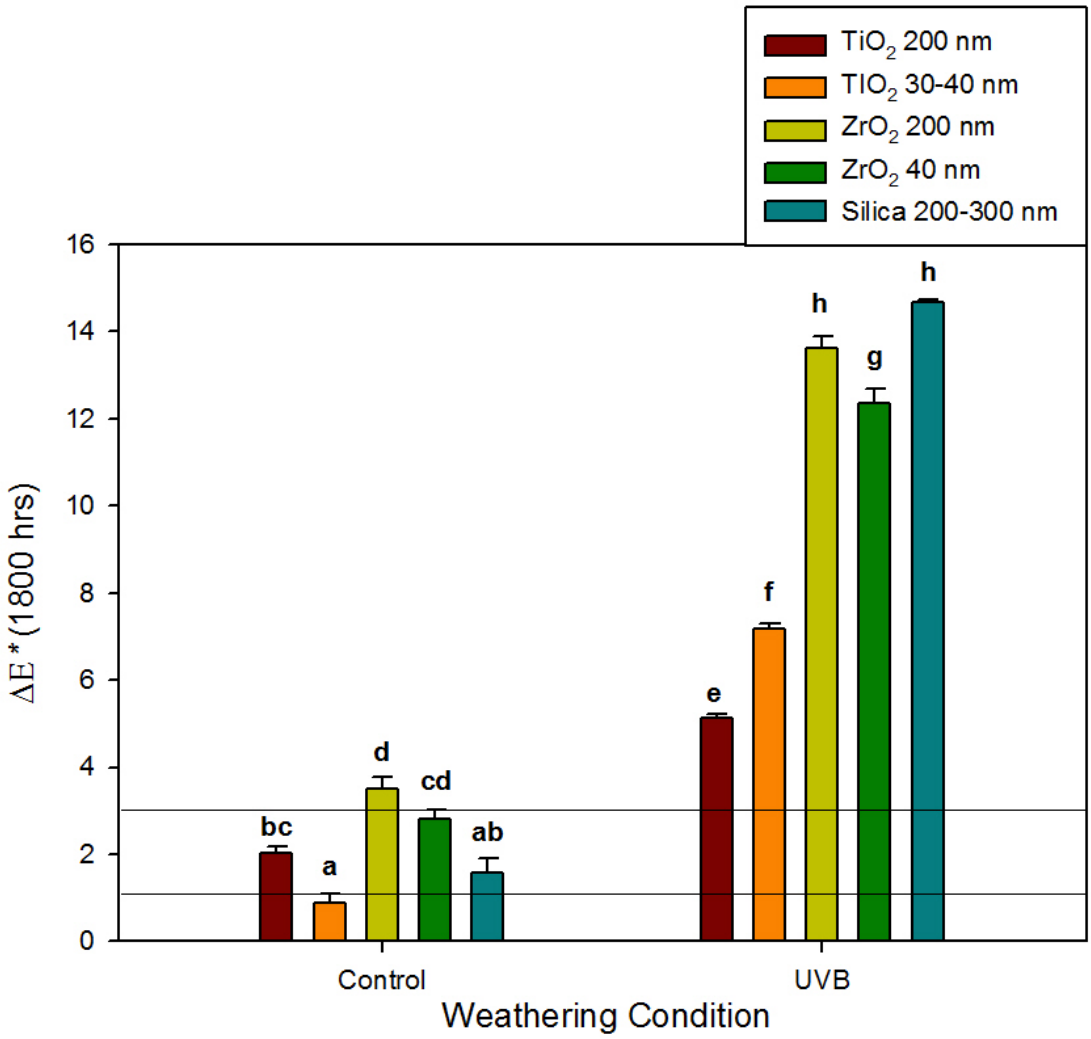

Figure 4.9. Bar graph displaying means and standard deviations (error bars) of ΔE* after 1800 hours of weathering for different groups (n=5). Means with the same lowercase letters are not significantly different ($p \geq 0.05$). Lines drawn at ΔE* = 1.1 and 3.0 represent the minimum thresholds for 50:50 visual perceptibility and acceptability, respectively.

results, 200 nm TiO_2 group had the lowest color change, which was followed by 30-40 nm TiO_2, 40 nm ZrO_2, and 200 nm ZrO_2 groups respectively ($p<0.05$, Fig 4.9). All groups were well above the acceptable color change threshold.

4.1.3 After 3000 Hours of Weathering

ΔL* results after 3000 hours' storage in control conditions showed that 30-40 nm TiO_2 and silica were the most positive (whiter), which and that was significant when compared to the ZrO_2 groups ($p<0.05$, Fig 4.10). ΔL* values for the 200 nm ZrO_2 group were the lowest (more negative, darker), which was significant only when compared to TiO_2 groups and the silica group ($p<0.05$, Fig 4.10). Under UVB weathering, the 200 nm TiO_2 group was the least negative (least darkest) followed by 30-40 nm TiO_2, 40 nm ZrO_2, 200 nm ZrO_2, and silica, respectively. All differences were statistically significant ($p<0.05$, Fig 4.10).

The red-green color parameter, Δa*, showed no significant differences among groups under control weathering conditions ($p>0.05$, Fig 4.11). For UVB weathering, the silica group showed the highest Δa* value (most red, meaning the highest amount of green fading) but no statistical significance was demonstrated among the groups ($p\geq0.05$, Fig 4.11).

For Δb* values after 3000 hours of control weathering, TiO_2 groups were the highest (most yellow), but no statistical significance was observed among the groups ($p\geq0.05$, Fig 4.12). Δb* values after 3000 hours of UVB weathering was the highest for TiO_2 (least amount of yellow fading), which was statistically significant only when compared to the silica group ($p<0.05$, Fig 4.12).

Table 4.4. ΔL*, Δa*, Δb* and ΔE* values after 3000 hours of weathering (Mean (S.D.), n=5)

Color Parameter	TiO_2 200 nm	TiO_2 30-40 nm	ZrO_2 200 nm	ZrO_2 40 nm	Silica 200-300 nm
ΔL*					
Control	-1.13 (0.14)	-0.61 (0.07)	-1.68 (0.06)	-1.43 (0.08)	-0.99 (0.08)
UVB	-3.13 (0.01)	-4.27 (0.07)	-8.50 (0.12)	-7.97 (0.10)	-10.82 (0.13)
Δa*					
Control	-0.27 (0.38)	0.06 (0.42)	-0.39 (0.66)	-0.25 (0.66)	0.44 (0.90)
UVB	1.20 (0.25)	1.27 (0.50)	1.70 (0.52)	1.62 (0.65)	3.23 (1.01)
Δb*					
Control	-2.48 (0.63)	-2.21 (1.26)	-5.85 (2.10)	-5.18 (2.10)	-5.00 (3.20)
UVB	-4.30 (0.84)	-6.28 (1.02)	-11.49 (2.57)	-11.89 (2.04)	-15.12 (3.03)
ΔE*					
Control	2.88 (0.59)	2.49 (1.24)	6.32 (2.05)	5.61 (2.06)	5.39 (3.21)
UVB	5.61 (0.59)	7.87 (0.81)	14.98 (1.61)	14.74 (1.47)	19.51 (2.01)

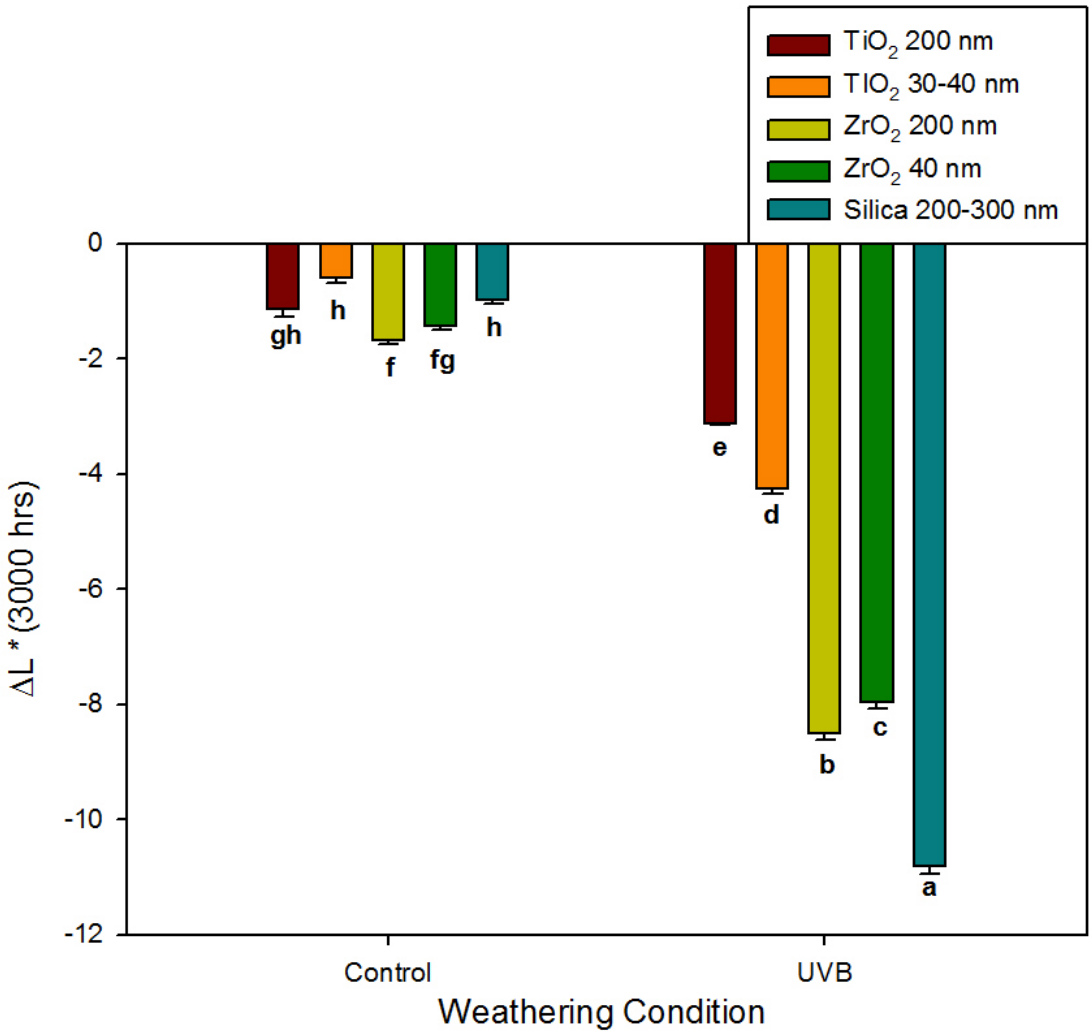

Figure 4.10. Bar graph displaying means and standard deviations (error bars) of ΔL* after 3000 hours weathering for different groups (n=5). Means with the same lowercase letters are not significantly different ($p \geq 0.05$).

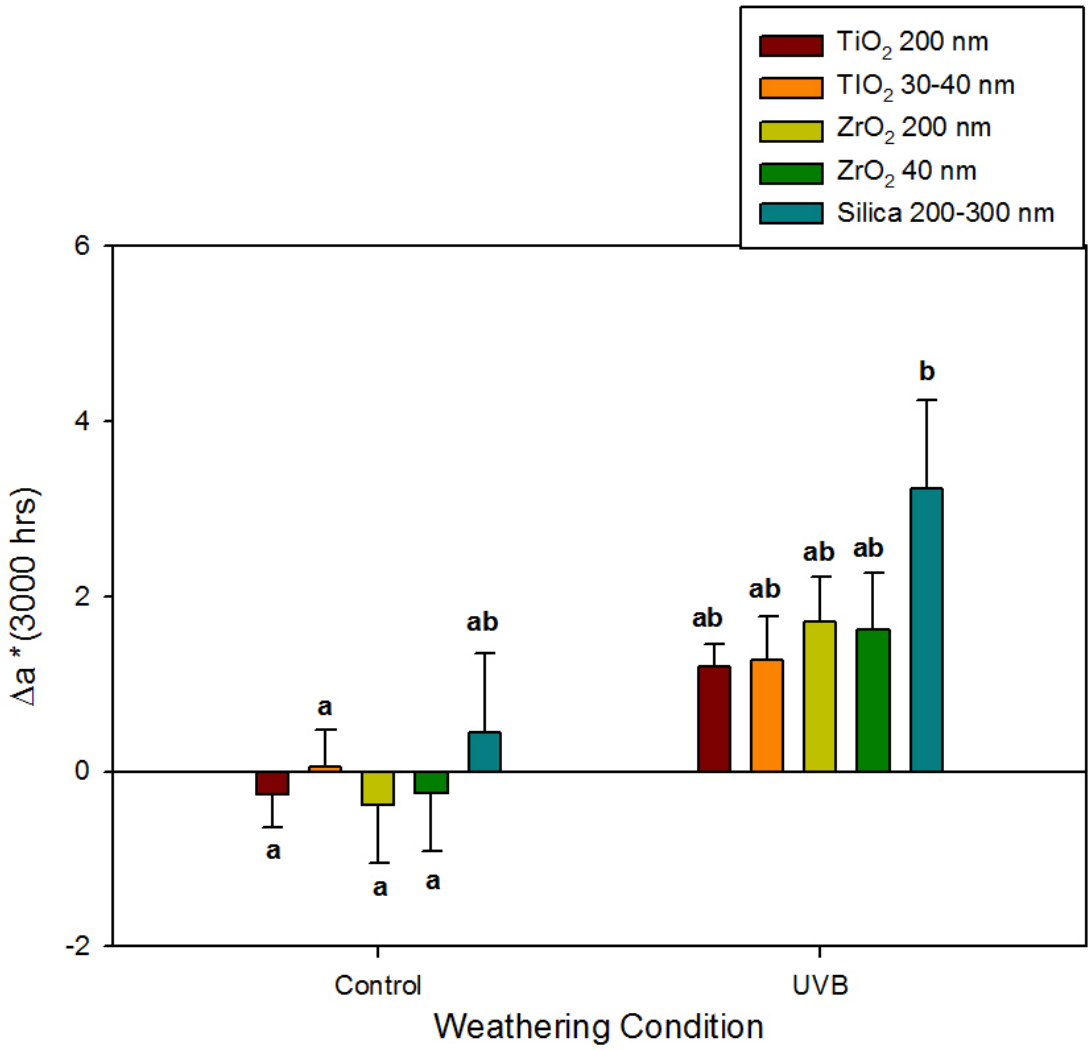

Figure 4.11. Bar graph displaying means and standard deviations (error bars) of Δa* after 3000 hours weathering for different groups (n=5). Means with the same lowercase letters are not significantly different ($p \geq 0.05$).

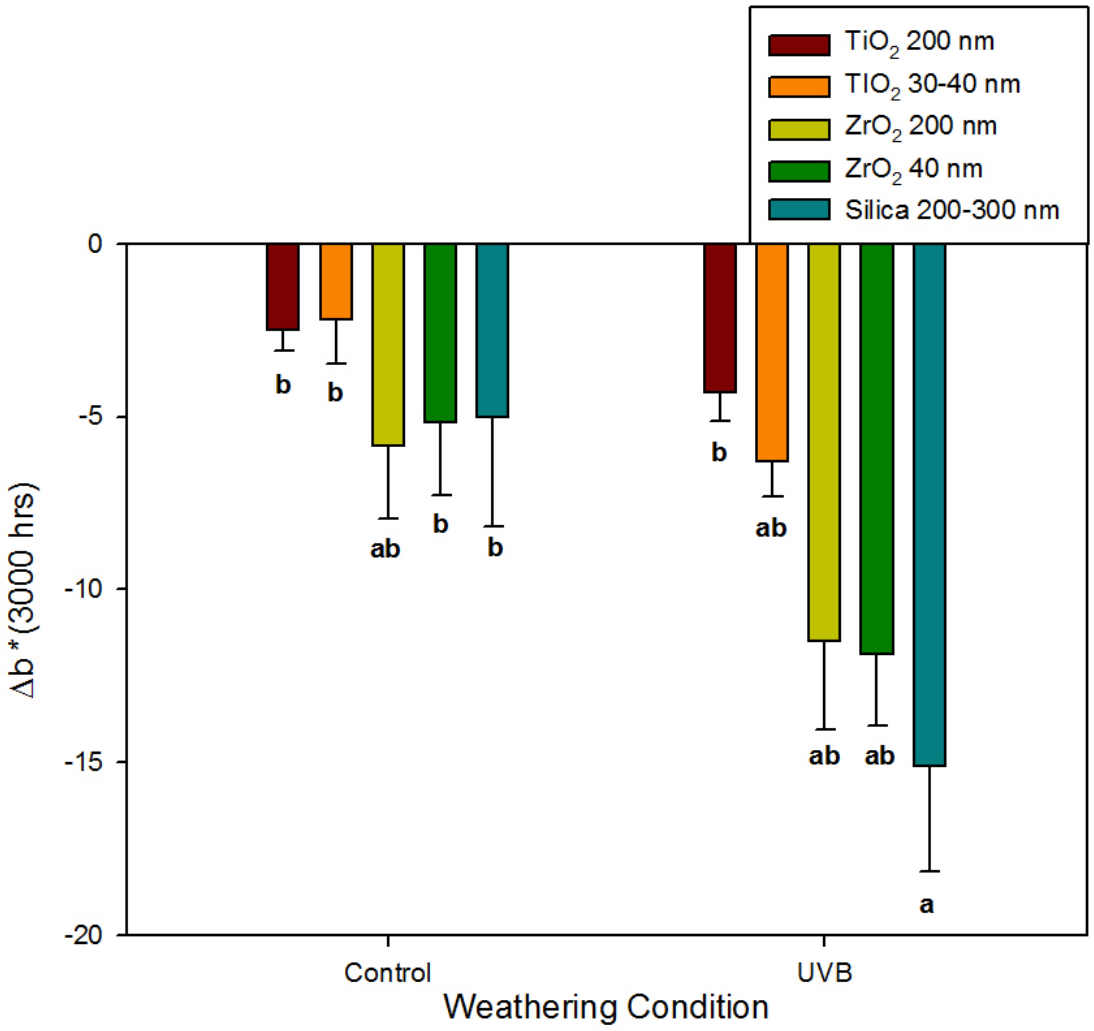

Figure 4.12. Bar graph displaying means and standard deviations (error bars) of Δb* after 3000 hours weathering for different groups (n=5). Means with the same lowercase letters are not significantly different ($p \geq 0.05$).

In observing the overall color change (ΔE*) after 3000 hours of control weathering, no statistical significant difference was demonstrated among all groups ($p \geq 0.05$, Fig 4.13). Only the TiO_2 groups demonstrated ΔE* values below the acceptable threshold of color change. After 3000 hours of UVB weathering, the 200 nm TiO_2 group showed the lowest color change, which was significant when compared to ZrO_2 groups and the silica group ($p<0.05$, Fig 4.13). The silica group showed the highest color change which was significant compared to TiO_2 groups ($p<0.05$, Fig 4.13). All groups had ΔE* values well above the acceptable level of color change.

A summary of ΔE* color change for each group in control and UVB weathering environments at each time interval (600 h, 1800 h, 3000 h) is shown in Fig 4.14. Generally color change increased over time, as UVB induced more color change for all groups at 600, 1800 and 3000 h compared to control weathering. The TiO_2 200 nm group displayed the lowest color change and silica group displayed the highest color change in control and UVB environments. Color change in control weathering was approximately at the same level at 600 h and 1800 h, then started to increase rapidly towards the 3000 h time point. This suggests that the PDMS samples were stable until after 1800 h of control weathering, then possible polymer and/or pigment degradation began to take place. UVB weathering induced higher increase in color change from 600 h to 1800 h followed by a slight increase reaching the 3000 h point. This can possibly be explained by initial pigment degradation from UVB exposure, followed by polymer degradation. Interestingly, error bars became larger after 3000 hours of weathering, suggesting that the materials were less stable at that time point.

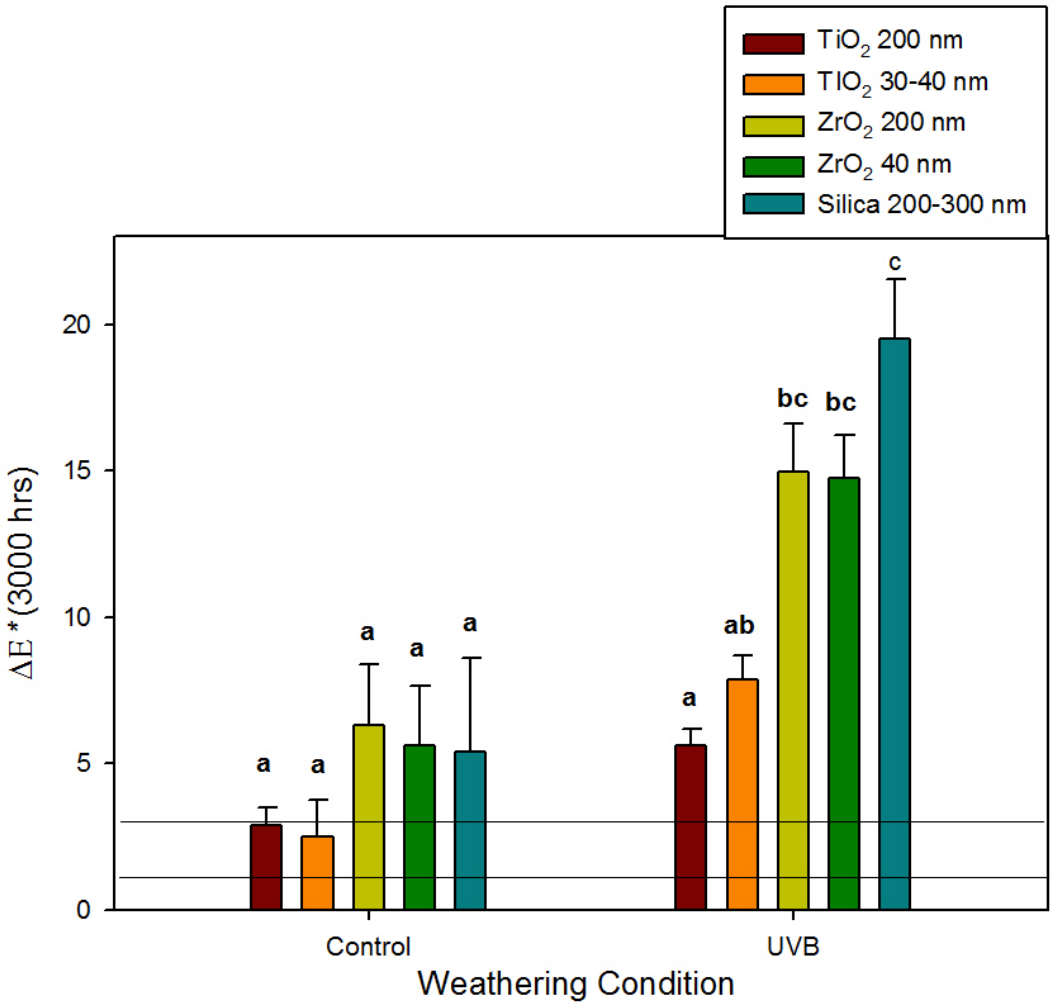

Figure 4.13. Bar graph displaying means and standard deviations (error bars) of ΔE* after 3000 hours weathering for different groups (n=5). Means with the same lowercase letters are not significantly different ($p \geq 0.05$). Lines drawn at ΔE* = 1.1 and 3.0 represent the minimum thresholds for 50:50 visual perceptibility and acceptability, respectively.

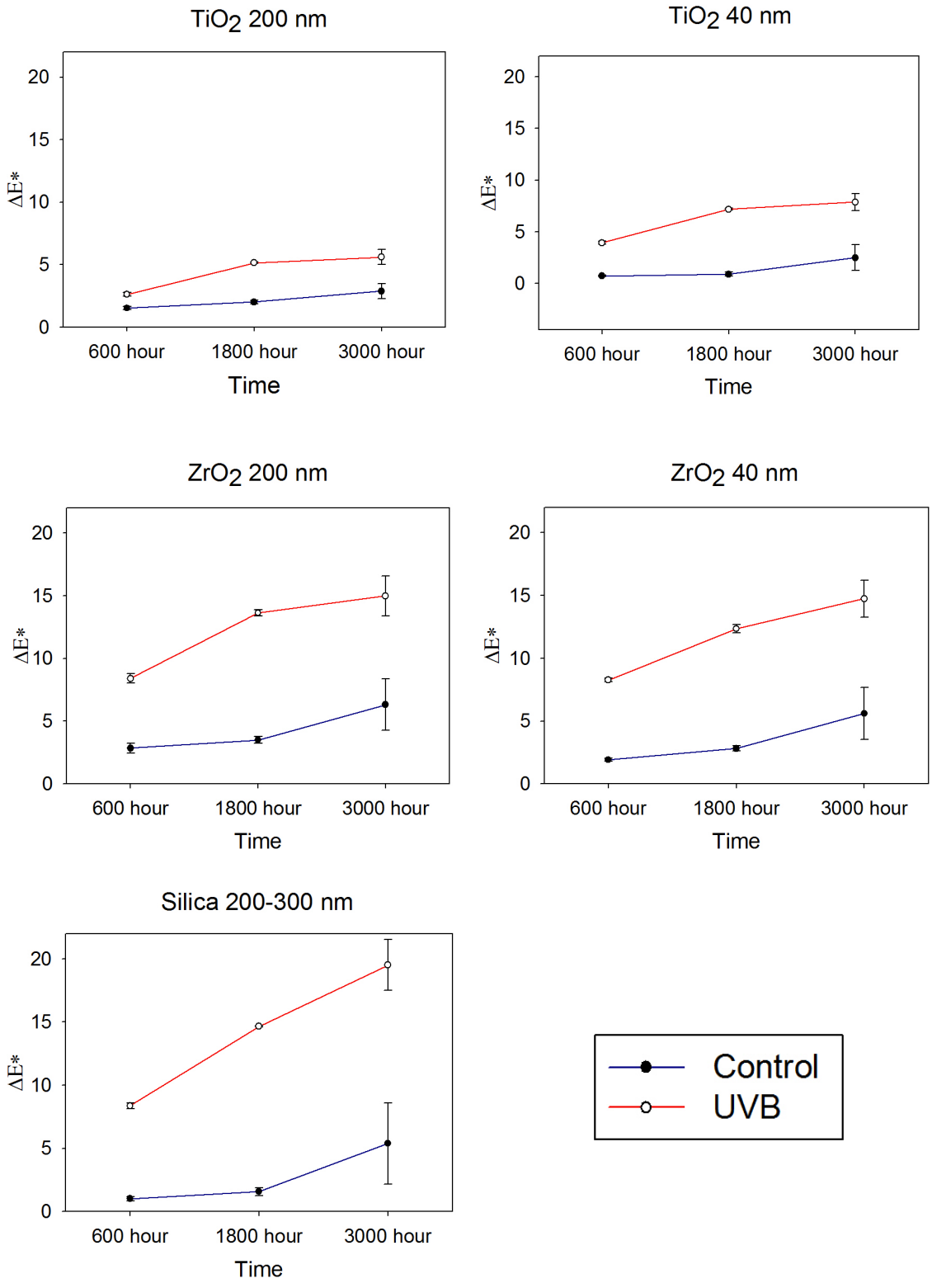

Figure 4.14. Line plots displaying means and standard deviations (error bars) of ΔE* over time (600, 1800 and 3000 hours).

4.2 Physical Properties

4.2.1 Shore A Hardness

Baseline shore A hardness values are presented in Fig 4.15. The silica group had higher hardness values than the other groups, which was statistically significant when compared to both TiO_2 groups and the 40 nm ZrO_2 group ($p<0.05$). It was not significant when compared to the 200 nm ZrO_2 group ($p\geq0.05$). The 200 nm ZrO_2 group showed an intermediate hardness values that was statistically higher than TiO_2 groups and the 40 nm ZrO_2 group ($p<0.05$). It should be pointed out that the silica group contained 13% weight filler loading compared to only 1% weight for the titania and zirconia groups.

After 3000 hours of weathering, the change in shore A hardness was minimal for the TiO_2 and ZrO_2 nanoparticle groups, ranging from -0.28 to +0.22 units with no significant differences detected among the nanoparticle groups in either control or UVB weathering environments (Fig 4.16). Compared to the other nanoparticle groups, the silica group showed a higher increase in hardness that was statistically significant, for both control and UVB weathering environments ($p<0.05$, Fig 4.16).

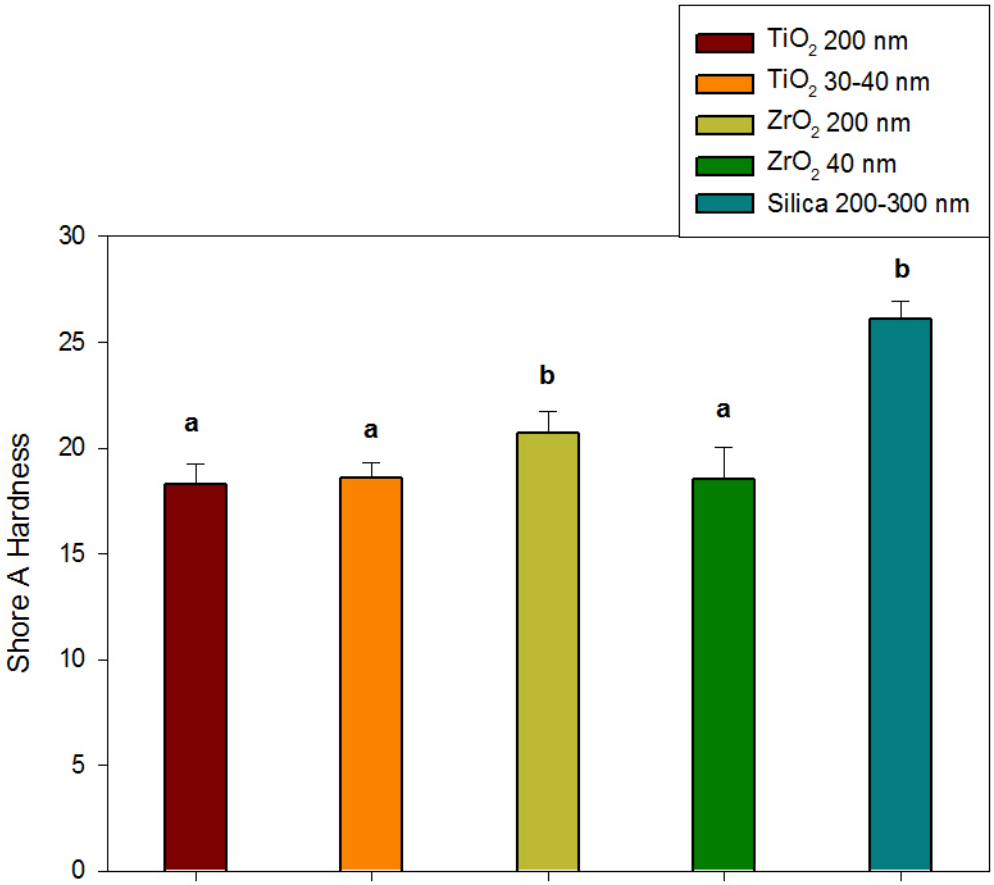

Figure 4.15. Bar graph displaying means and standard deviations (error bars) of baseline Shore A hardness (n=5). Means with the same lowercase letters are not significantly different ($p \geq 0.05$).

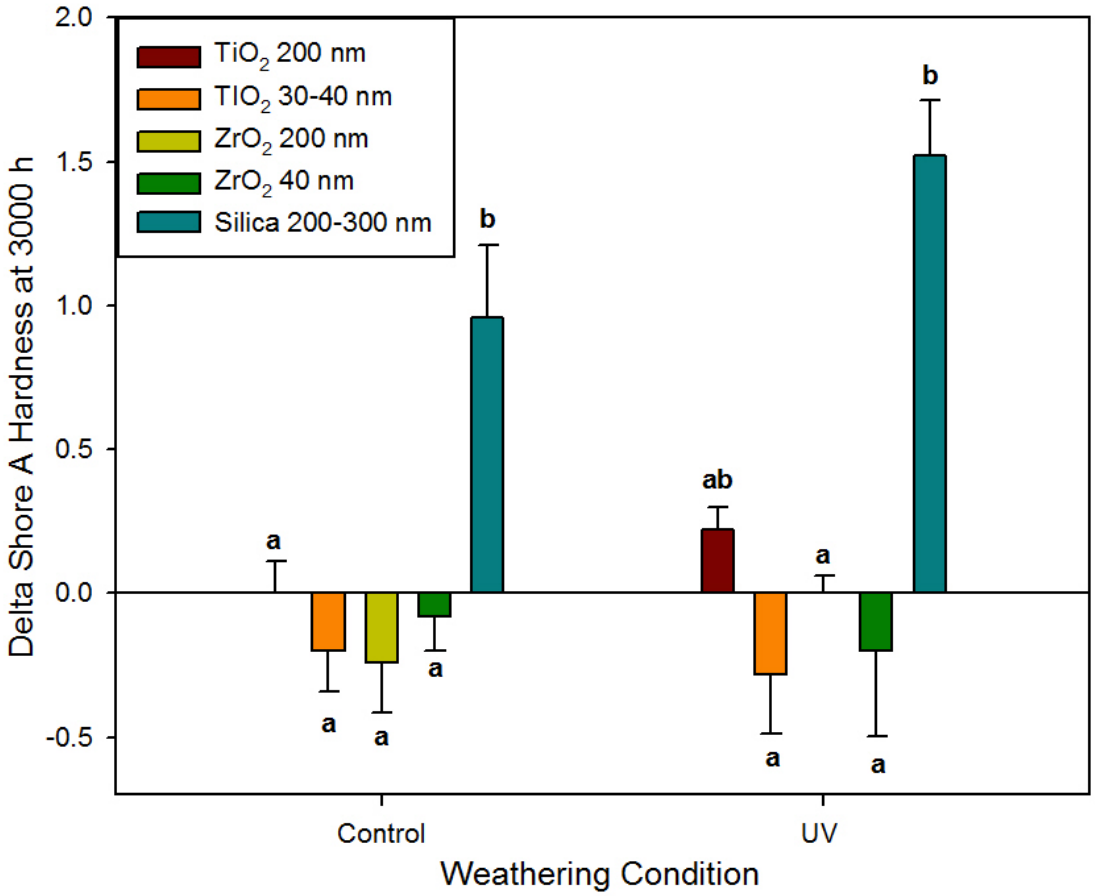

Figure 4.16. Bar graph displaying means and standard deviations (error bars) of delta Shore A hardness after 3000 hours of weathering (n=5). Means with the same lowercase letters are not significantly different ($p \geq 0.05$).

4.2.2 Tensile Properties

Mean ultimate tensile strength (UTS) values were significantly greater for the silica group, as compared to the TiO_2 and ZrO_2 groups for tests conducted immediately (baseline) and after 3000 hours' storage in control and UVB weathering conditions ($p<0.05$, Fig 4.17, Table 4.5). Immediate UTS values for the silica group were significantly greater when compared to those measured after control and UVB weathering ($p<0.05$, Fig 4.17, Table 4.5). The weathered groups were not significantly different from one another.

Modulus of elasticity was significantly greater for the silica group compared to the experimental groups at all time periods and weathering conditions ($p<0.05$, Fig 4.18, Table 4.5). No significant differences were observed among any of the experimental groups at any time or for any weathering condition ($p\geq0.05$, Fig 4.18, Table 4.5).

For the strain at break, silica groups were significantly greater than the experimental groups for all three testing conditions ($p<0.05$, Fig 4.19, Table 4.5). The immediate mean value of strain at break for ZrO_2 200 nm group was significantly lower than both TiO_2 groups. After 3000 hours of storage in control and UVB environments, the silica group showed mean strength values that were significantly lower than immediate mean values. For the experimental $TiO_2$and ZrO_2 groups, strain at break values showed minimal changes between the three testing conditions that were not statistically significant ($p\geq0.05$, Fig 4.19, Table 4.5).

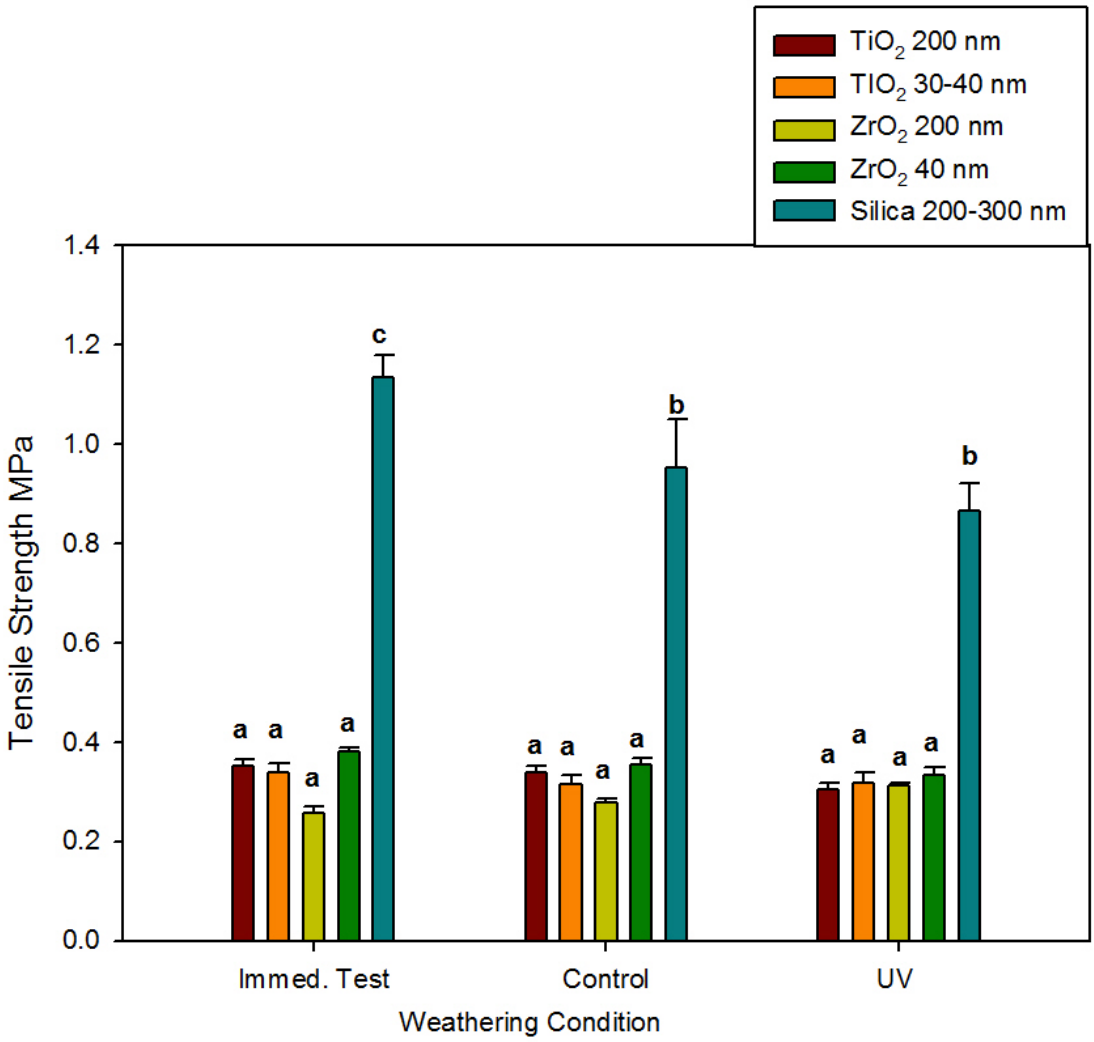

Figure 4.17. Bar graph displaying means and standard deviations (error bars) of ultimate tensile strength at baseline and after 3000 hours of weathering (n=12). Means with the same lowercase letters are not significantly different ($p \geq 0.05$).

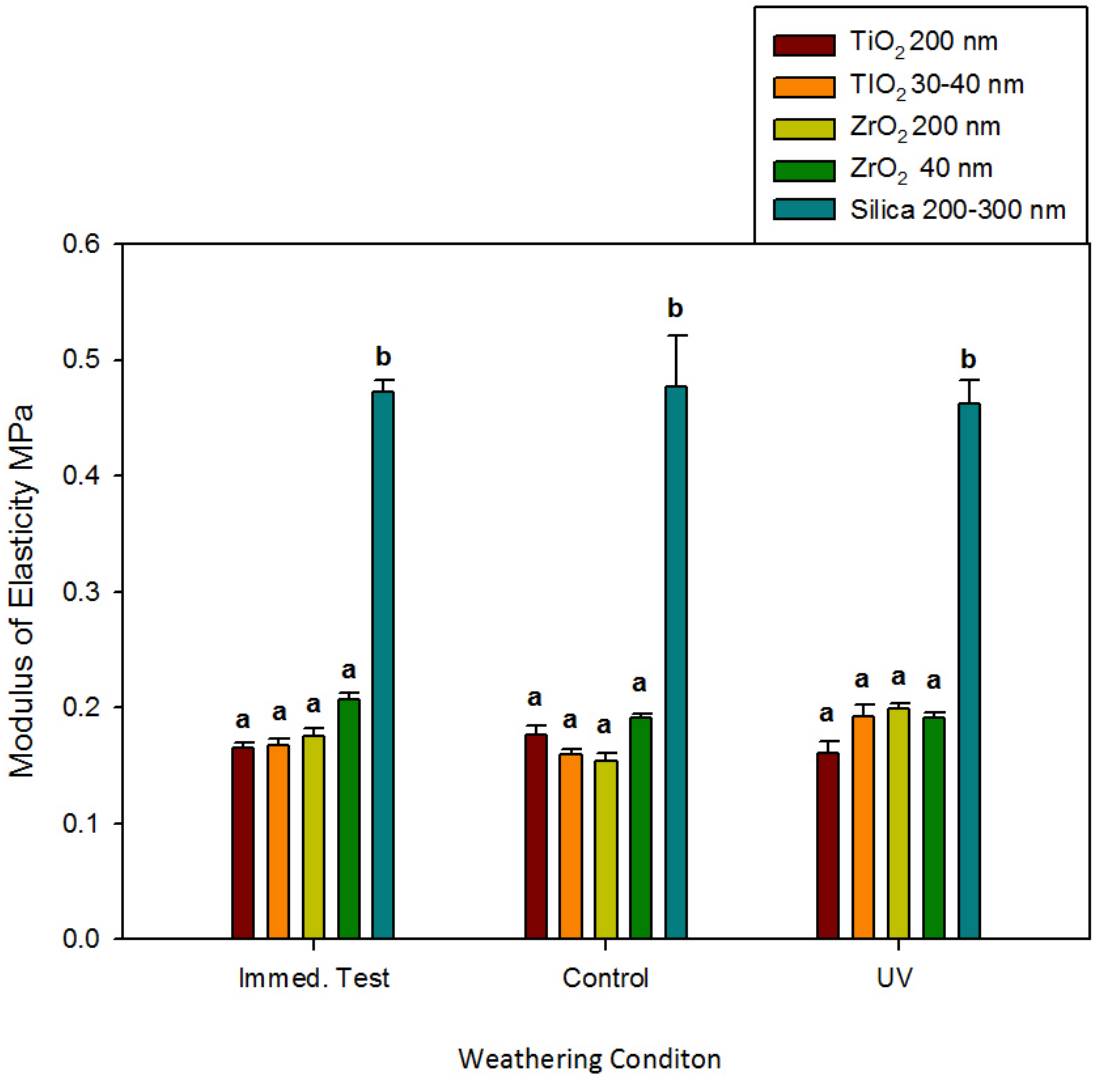

Figure 4.18. Bar graph displaying means and standard deviations (error bars) of modulus of elasticity at baseline and after 3000 hours of weathering (n=12). Means with the same lowercase letters are not significantly different ($p \geq 0.05$).

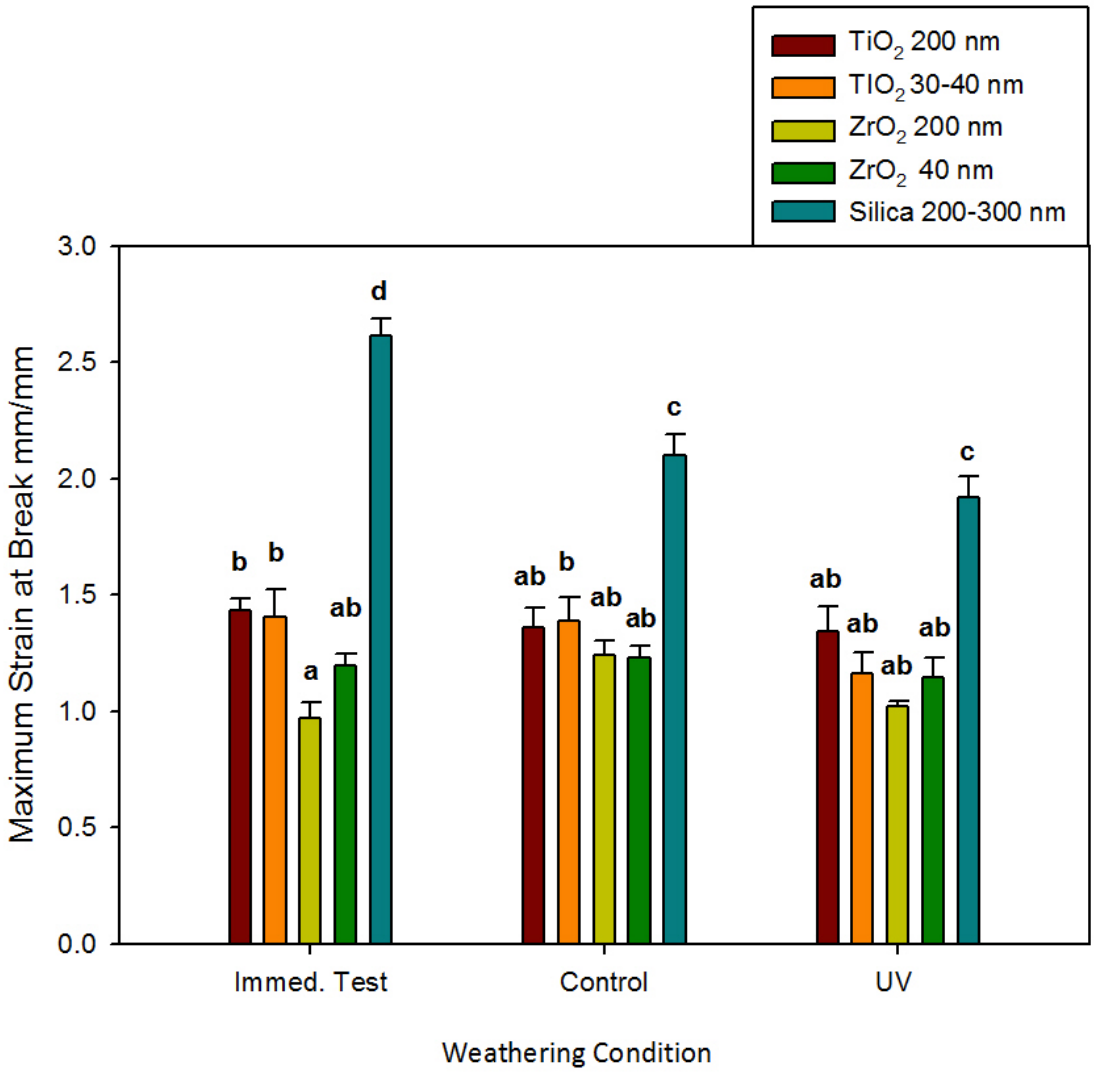

Figure 4.19. Bar graph displaying means and standard deviations (error bars) of strain at break at baseline and after 3000 hours of weathering (n=12). Means with the same lowercase letters are not significantly different ($p \geq 0.05$).

Table 4.5. Tensile Properties after 3000 hours of weathering (Mean (S.D.), n=12)

Tensile properties	Testing Condition	TiO_2 200 nm	TiO_2 30-40 nm	ZrO_2 200 nm	ZrO_2 40 nm	Silica 200-300 nm
Ultimate Tensile Strength (UTS)	Immediate	0.35 (0.01)	0.34 (0.02)	0.26 (0.01)	0.38 (0.01)	1.13 (0.04)
	Control	0.34 (0.01)	0.31 (0.02)	0.28 (0.01)	0.36 (0.01)	0.95 (0.10)
	UVB	0.30 (0.01)	0.32 (0.02)	0.31 (0.01)	0.33 (0.01)	0.87 (0.06)
Strain at Break	Immediate	1.43 (.05)	1.41 (0.11)	0.97 (0.07)	1.20 (0.05)	2.61 (0.07)
	Control	1.36 (0.09)	1.39 (0.10)	1.24 (0.07)	1.23 (0.05)	2.10 (0.09)
	UVB	1.35 (0.11)	1.16 (0.09)	1.02 (0.02)	1.15 (0.08)	1.92 (0.09)
Modulus of Elasticity	Immediate	0.17 (0.00)	0.17 (0.01)	0.18 (0.01)	0.21 (0.00)	0.47 (0.01)
	Control	0.18 (0.01)	0.16 (0.00)	0.15 (0.01)	0.19 (0.00)	0.48 (0.04)
	UVB	0.16 (0.01)	0.19 (0.01)	0.20 (0.01)	0.19 (0.01)	0.46 (0.02)

4.3 Antifungal Activity

4.3.1 XTT Colorimetric Assay

The optical density of formazan crystal formation in solution was measured spectrophotometrically at 492 nm after 48 hours of exposure to *C. albicans*. This was a measure of metabolic activity (Fig 4.20, Table 4.6). Ag and TiO_2 nanoparticle groups showed significantly lower *C. albicans* metabolic activity when compared to the positive control group ($p<0.01$). The ZrO_2 and silica groups were not significantly different than the positive control group ($p\geq0.01$).

4.3.2 Confocal Laser Scanning Microscopy (CLSM)

Fun-1 staining showed that *C. albicans* biofilm formation is a complex phenomenon. The biofilm was multiple cells layers in thickness consisting mainly of yeast and hyphae. Adjacent to the silicon elastomer disc surface, yeast cells were densely embedded in an extracellular matrix. In both Ag groups and TiO_2 200 nm groups, confocal laser microscopy images showed yeast cells scattered and attached to the elastomer discs with no hyphae formation detected. Pseudohyphae and more yeast cells with extracellular networks were detected in TiO_2 30-40 nm group images and more dense and thick mature hyphae process formations were noticed in ZrO_2 and silica groups (Fig 4.21).

Table 4.6. *C.albicans* Metabolic Activity after 48 hours Measured Spectrophotometrically at 492 nm (Mean (S.D.), n=9 for silica and nanoparticle groups, n=12 for positive control)

Group	XTT after 48 h
Ag 200-400 nm	0.31 (0.07)
Ag 30-40 nm	0.31 (.04)
TiO_2 200 nm	0.33 (0.25)
TiO_2 30-40	0.70 (0.23)
ZrO_2 200	1.00 (0.16)
ZrO_2 40	1.01 (0.12)
Silica 200-300 nm	1.13 (0.11)
Positive control	1.17 (0.00)

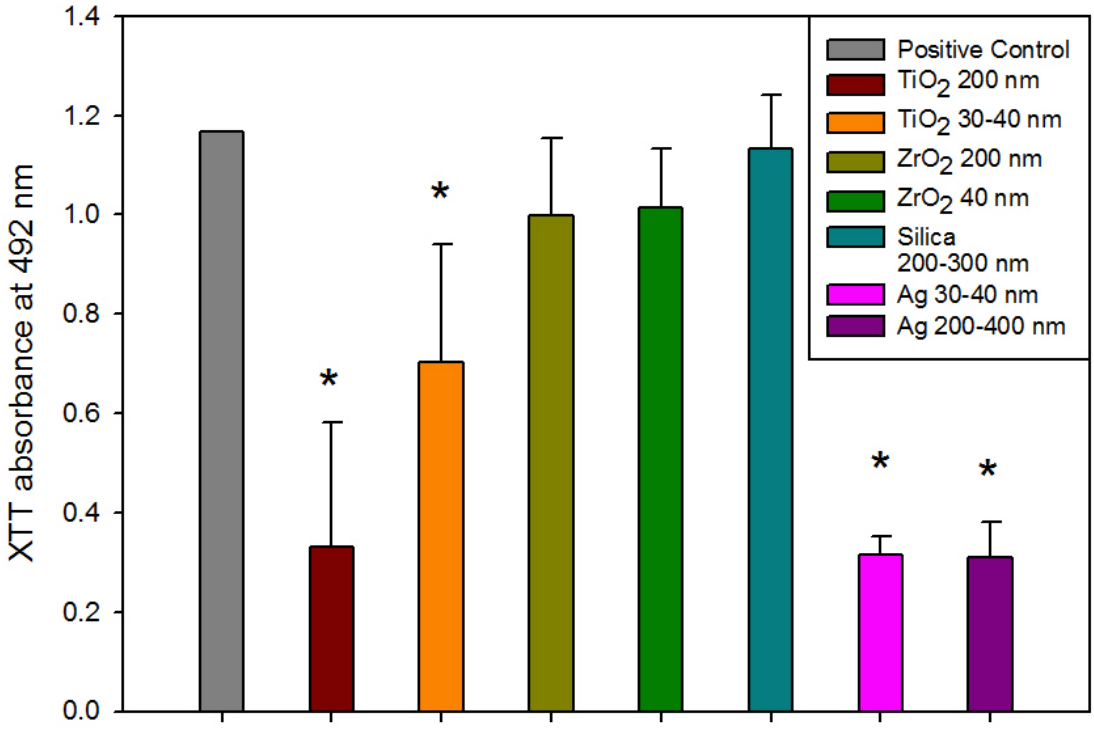

Figure 4.20. Bar graph displaying means and standard deviations (error bars) of *C. albicans* optical density measured spectrophotometrically at 492 nm after 48 hours. Asterisk denotes significant difference from positive control ($p<0.01$).

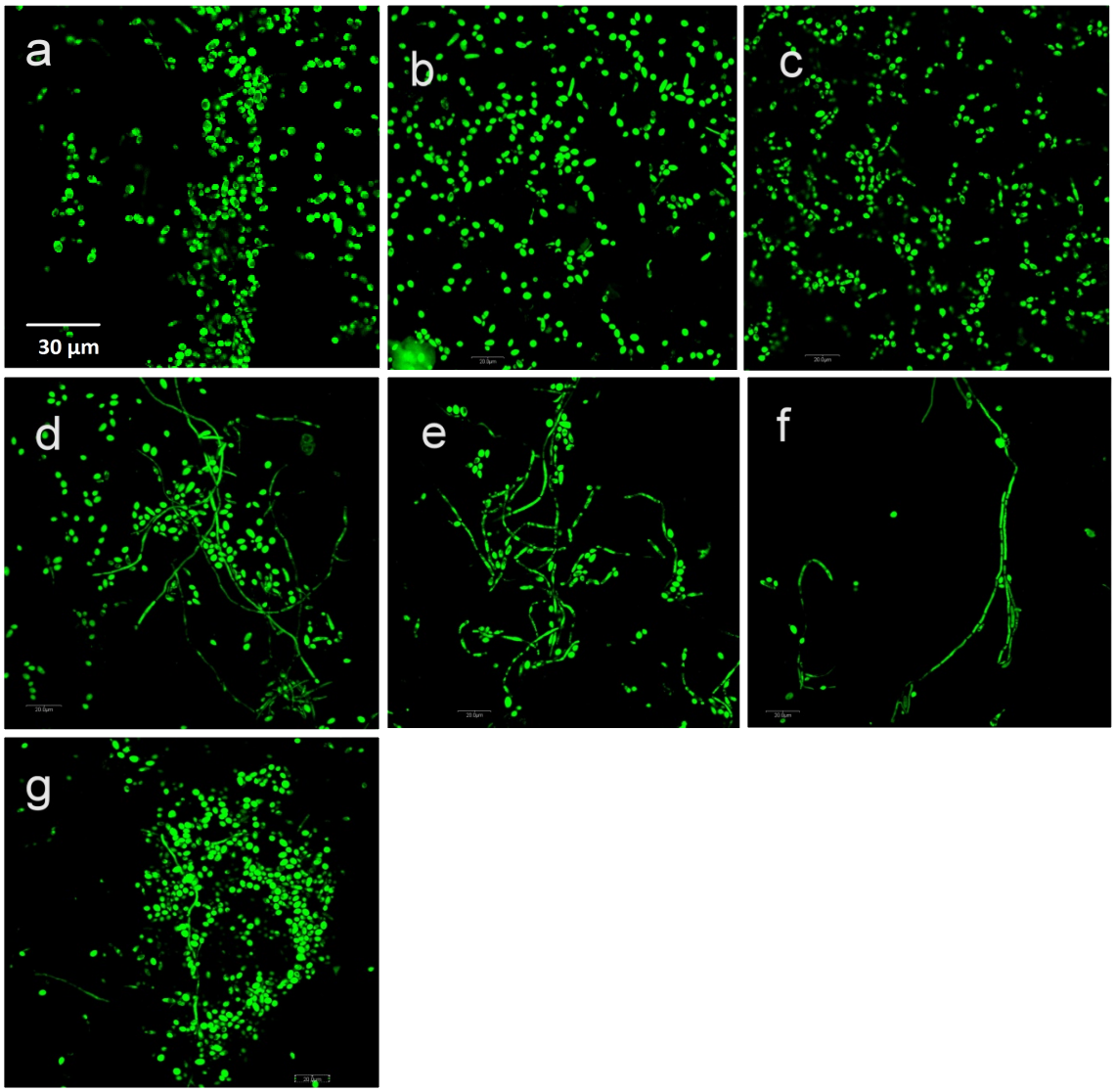

Figure 4.21. Confocal laser scanning micrographs of *C. albicans* stained with FUN-1. a) Ag 200-400 nm. b) Ag 30-40 nm. c) TiO_2 200 nm. d) TiO_2 30-40 nm. e) ZrO_2 200 nm. f) ZrO_2 40 nm. g) Silica 200-300 nm. Magnification 40x, oil. Scale bar = 30 μm.

CHAPTER 5: DISCUSSION

The central hypothesis of this study was that the addition of TiO_2 and ZrO_2 nanoparticles to pigmented PDMS elastomers would improve color stability and physical properties when subjected to controlled dosages of ultraviolet radiation. The results of this investigation demonstrated that TiO_2 nanoparticles improved color stability, but ZrO_2 did not. Neither nanoparticle improved physical properties when added at 1% by weight. The second hypothesis was that *C. albicans* growth on the surface of pigmented PDMS elastomers would be reduced by addition of TiO_2 and ZrO_2 nanoparticles. The results demonstrated that TiO_2 nanoparticles permitted less biofilm growth than did silica particles, but ZrO_2 did not. Interpretations of results are presented in the following sections.

5.1 Color Change

5.1.1 Color Changes at Baseline

TiO_2 nanoparticle additions caused noticeable visual color change at baseline as compared to silica controls. TiO_2 produced samples which were lighter in color compared to silica controls (L* values ranging 88-90 for TiO_2 and 79 for silica). On the other hand, ZrO_2 groups produced samples with similar L* values as compared to silica-filled samples (both near L*=79). Color is the result of the interaction of the pigment color, nanoparticle size and the relative difference between the refractive indices of the nanoparticle and the polymer. The refractive index of TiO_2 is more than 2.6 whereas ZrO_2 is about 2.1, Silica is about 1.5 and PDMS is around 1.4. Generally, light is bent more, travels shorter paths and does not penetrate as deeply in materials with higher refractive indices. Therefore, samples containing TiO_2 are more efficient at scattering light than are the other groups, leaving smaller amounts of light to be absorbed by the polymer and the pigment. The scattering effect of TiO_2 nanoparticles gives the samples a

whiter appearance, thereby explaining higher L* values. Small, non-significant changes were measured in a* (red-green), which was somewhat expected since the pigment was yellow in color. For b* values, silica filled samples produced the highest yellow color (b*=93.18) which was statistically grouped with ZrO_2 samples (b* values were 88.76 for ZrO_2 200 nm and 91.48 for ZrO_2 40 nm samples). The whiteness contributed by TiO_2 presumably detracted from the yellow color and yielded lower b* values (55.60 for TiO_2 200 nm and 60.06 for TiO_2 30-40 nm).

5.1.2 Color Changes in Control Environment

In the control environment (darkness, 25℃, and 30% relative humidity), more overall color change was noticed for ZrO_2 groups and the silica-filled samples after 3000 hours of storage, as compared to TiO_2-containing materials ($p < 0.05$). This may be attributed to pigment breakdown, detachment of filler particles, degradation of the lower molecular weight silicon fluid used to disperse the platinum catalyst, presence of impurities or continued crosslinking of the matrix. Additional crosslinking occurs when unreacted chains continue to polymerize with time, thereby changing the refractive index of the polymer. Elastomers containing both TiO_2 sizes underwent a mean color change that was below the visual threshold of acceptable color change ($\Delta E^*=3$). The lower overall color change noticed with TiO_2 may be due to its higher specific heat, which may allow more heat transmission to the polymer, possibly inducing more polymerization during the curing process and thereby reducing post-curing polymerization. Post-curing polymerization may have produced the color changes noted for silica and zirconia. However, the true underlying mechanism is unknown.

5.1.3 Color Change Caused by Ultraviolet Radiation

Early studies demonstrated that ultraviolet radiation negatively impacted optical and mechanical properties in maxillofacial prosthetic materials. A common explanation given for these changes is that oxygen, when present, induces photo-oxidative degradation of the polymer network in addition to the degradation of non UV-resistant pigments. Results from UVB weathering showed that TiO_2 200 nm samples demonstrated the least color change over time, followed by TiO_2 30-40 nm samples. This suggests that 200 nm TiO_2 nanoparticles functioned as UVB blockers, thereby reducing ultraviolet transmission to surrounding pigment and polymer molecules. The difference in UV blocking capabilities between the two TiO_2 groups may be attributed to the difference in the size of the scattering particles. For the 200 nm TiO_2 nanoparticles whose diameter is closer to one-half the wavelength produced by the ultraviolet bulb (290-315 nm), the Mie scattering theory is applicable and more forward scattering will be produced closer to the peak of the total scattering intensity. On the other hand, the smaller 30-40 nm particles may more closely follow the Rayleigh scattering theory, which shows that small particles produce equal amounts of backward and forward scattering. In principle, the 200 nm particle would produce more forward scattering, whereas the 30-40 nm particle would permit more backward (diffuse) scattering to the surrounding polymer and pigment. This, in turn, would lead to material degradation within a shorter period of time. It should be pointed out that although the ΔE^* value for TiO_2 200 nm was 5.6 units after 3000 hours of UVB exposure and above the acceptable threshold of color change ($\Delta E = 3.0$), this degree of color change may not be unacceptable to some observers. It should be noted that the measurement used to determine the perceptibility and acceptability thresholds of color difference was determined from Paravina et al., where color measurements of different skin-colored elastomers were evaluated in a viewing booth with neutral gray walls and a floor which lowered the visual

lightness threshold (2009). These thresholds might not fully represent a maxillofacial prosthesis that is viewed under different light sources and with different backgrounds. Also, a patient might not reject a facial appliance with minimal shade change as long as the change occurs gradually.

Based on our results, improvements in color stability were obtained by adding 1% weight TiO_2 nanoparticles to silicon elastomers exposed to artificial weathering, which is consistent with findings reported by Han et al., 2010. For 1% TiO_2 incorporated into Silicone A-2186 with yellow pigments and exposure to artificial solar radiation (450 kJ/m^2), ΔE^* was measured at 5.2 units. Color stability improved with samples containing higher concentrations of TiO_2 (2% to 2.5%) and mixed pigments, rather than one pigment.

5.2 Physical Properties

5.2.1 Shore A Hardness

Baseline shore A hardness showed that silica was superior to all other groups except the 200 nm ZrO_2 group. The fact that the 1% nano-oxide additions were only slightly lower in hardness to the 10% silica additions may be explained by considering the nature of the polymer reinforcing behavior of nanoparticles when dispersed into silicone. Hardness is a surface phenomenon and is affected by the surface area of incorporated filler. The large total surface area of smaller particles may underlie the observation that 1% TiO_2 and ZrO_2 30 nm particles yielded similar hardness values to those measured for control materials containing 13% 200 nm silica particles. The surface area/weight ratio increases by one to two orders of magnitude as the nanoparticle decreases in size to 10 nm (Rothon 2003).

Overall there were few differences in Shore A hardness observed among the different

materials, and only silica-filled elastomers demonstrated appreciable hardening from weathering. The 1.5 unit increase in hardness was considered to be clinically insignificant.

5.2.2 Tensile Properties

Compared to the TiO_2- and ZrO_2-filled samples, ultimate tensile strength, maximum strain at break and modulus of elasticity were significantly greater for the silica-filled elastomers at all time points for both control and UVB weathering (roughly 2-3 times greater UTS, 2 times maximum strain and 2-3 times greater modulus). This was probably due to the increased filler loading for silica-containing materials. Increasing filler levels have been shown to increase mechanical properties for micrometer-range fillers loaded into polymer systems. In this study, it was considered possible that ten-fold lower filler sizes loaded in ten-fold lower quantities might produce similar mechanical properties to materials loaded with larger fillers in larger quantities. This consideration was based on wear data published by Bahadur and Gong and mechanical property data published by Sinha and Brisco. Similar results were not observed in this study because wear is a more complex phenomena that is accompanied by compressive and shear stress, which is different than the tensile behavior of the material. Wear can occur in adhesive, abrasive and fatigue modes and require surface contact. Thus, it is possible that nano-filled materials may exhibit different behavior under tensile stress.

TiO_2- and ZrO_2-nanoparticle-filled samples' tensile properties were not significantly affected by weathering condition. This result should be regarded with caution, as property values were inherently low initially. This might be due to the low filler content used in this study, which did not raise the mechanical properties sufficiently to permit weathering changes to be observed. Similar findings were reported by Han et al., 2008. They concluded that the incorporation of 0.5%, 1% and 1.5% loading fraction did not improve mechanical properties,

whereas 2-2.5% of TiO_2, ZnO and CeO_2 did improve tensile and shear strength, maximum elongation at break and Shore A hardness. However their results are not directly comparable to our findings, since they incorporated nanoparticles into Silicon A-2186, a commercial elastomer that contains silica in addition to the loaded nanoparticles. In this study, prototype elastomers containing only nano-oxides were tested.

Ultimate tensile strength (UTS) and maximum strain at break of silica-filled samples was significantly decreased by time passage (control) and UVB radiation, but there were no significant differences between control and UVB weathering. Changes from baseline may be attributed to continued crosslinking and chain scission within the polymer network over time; however this effect was not increased by UVB exposure. The modulus of elasticity for silica samples was not affected by time passage or UVB exposure. The reason for this occurrence is unclear.

5.3 Antifungal Activity

Candida albicans are opportunistic fungi that have to overcome the host's immune system in order to produce an infection. Its ability to change from yeast cells to hyphal cells is known to be one of its virulent factors. *C. albicans* biofilm development is characterized by three distinct phases. The first is the adherence of *C. albicans* to its substrate (≈ 0-11 hours). In the intermediate phase, cell proliferation and microcolony formation takes place and deposits an extracellular matrix (≈ 12-14 hours). Finally, the formation of a dense network of filamentous forms (pseudohyphae and hyphae) encased in exopolymeric matrix is considered the maturation phase (≈ 24-72 hours) (Chandra et al., 2001, Alsalleeh et al., 2016). For this reason, *C. albicans* were incubated for 48 hours before conducting the XTT colorimetric assay and confocal laser

scanning microscopy experiments, to allow for the biofilm formation to reach its maturation phase.

Results from the XTT colorimetric assay showed that TiO_2 groups demonstrated similar antifungal activity to Ag (negative material control) with significantly less *C. albicans* growth compared to the positive control. The precise mechanism by which Ag and TiO_2 may control the growth of *C. albicans* is not fully understood. Early studies have shown that Ag ions block microbial DNA replication, inactivate vital enzymes necessary for ATP production and oxidation of glucose, and damage microbial cell walls, resulting in cell death (Allaker 2010). Similar effects have been suggested for TiO_2, as it oxidates the cell membrane of the microorganism and alters Coenzyme A-dependent enzyme activities, thereby producing a biocidal effect. The proposed mechanism is through the formation of reactive OH^- and HO_2^- species, the result of Ti-O surface bonds produced by mismatches between bulk and surface electronic properties (Longo et al., 2013). No significant differences were noticed between ZrO_2 and silica groups when compared to the positive control. Consequently, *C. albicans* grew and formed more hyphae on ZrO_2 and silica discs, as seen in confocal images. The poor antifungal activity of ZrO_2 and silica could be due to the lack of ability to produce free reactive radicals that can attack candidal cell walls and essential enzymes. Therefore, TiO_2 nanoparticles were able to limit *C. albicans* cells growth on the surface of PDMS discs, but ZrO_2 and SiO_2 did not.

CHAPTER 6: CONCLUSIONS

The purpose of this study was to compare elastomers filled with 1% weight TiO_2 and ZrO_2 nanoparticles in two particle sizes (40 nm and 200 nm) to elastomers filled with 13% weight silica nanoparticles, to evaluate of color stability and physical properties after exposure to control and UVB weathering challenges. A second purpose was to analyze the antifungal properties of these same PDMS elastomers. Conclusions of this study are as follow:

1. PDMS elastomers loaded with 1% weight 200 nm and 40 nm TiO_2 nanoparticles demonstrated less overall color change after storage in control ($p<0.05$) and UVB ($p<0.05$) environments compared to samples filled with ZrO_2 and silica nanoparticles.

2. Elastomers filled with 13% silica showed higher shore A hardness at baseline ($p<0.05$) compared to all other groups, except samples filled with 200 nm ZrO_2 nanoparticles. Weathering only affected samples filled with silica, producing a 1.5 hardness unit's increase, which was considered to be clinically insignificant.

3. Tensile properties of ultimate tensile strength UTS, maximum strain at break and modulus of elasticity were significantly higher for silica samples in immediate testing ($p<0.05$), control ($p<0.05$) and UVB ($p<0.05$) weathering environments, compared to all other groups.

4. Incorporation of 1% loading weight TiO_2 nanoparticles into PDMS imparted greater antifungal activity ($p<0.01$) compared to ZrO_2 and silica-filled samples.

CHAPTER 7: RESEARCH LIMITATIONS

The limitations associated with this project include the following:

1. Analysis of other weathering environments such as heat and humidity and using outdoor weathering would provide further insight into this project.

2. Only one pigment (functional intrinsic yellow) was chosen for this study. Different pigments would produce different behaviors of studied materials.

3. Prototype elastomers were used in this project in order to control their compositions precisely. Commercially available elastomers may behave in a different manner.

CHAPTER 8: CONSIDERATIONS FOR FUTURE RESEARCH

Results of this study suggest investigating the effects of adding similar levels of loading of TiO_2, ZrO_2, and silica nanoparticles into PDMS elastomers to allow for direct comparison between them.

Another consideration is to study the effects of adding a combination of different nanoparticles into PDMS elastomers at controlled compositions, which may produce more desirable properties.

Outdoor weathering may produce different material performance, therefore outdoor weathering should be considered as a future environmental challenge.

The dispersion of the nanoparticles when loaded into PDMS elastomers is an essential factor in obtaining the optimal properties of materials. Future research should focus on particle surface coatings that produce uniform particle spacing.

Finally, the effect of weathering on long-term antifungal activity of PDMS elastomers should be studied.

REFERENCES

Abdelsayed V, Alsharaeh E, El-Shall MS (2006). Catalyzed radical polymerization of styrene vapor on nanoparticle surfaces and the incorporation of metal and metal oxide nanoparticles within polystyrene polymers. Journal of Physical Chemistry B 110(39):19100-19103.

Ahn SJ, Lee SJ, Kook JK, Lim BS (2009). Experimental antimicrobial orthodontic adhesives using nanofillers and silver nanoparticles. Dental Materials 25(2): 206-213.

Allaker RP (2010). The use of nanoparticles to control oral biofilm formation. Journal of Dental Research 89(11):1175-1186.

Allaker RP, Ren G (2008). Potential impact of nanotechnology on the control of infectious diseases. Transactions of the Royal Society of Tropical Medicine and Hygiene 102(1): 1-2.

Allen NS, Edge M, Ortega A, Liauw CM, Stratton J, McIntyre RB (2002). Behaviour of nanoparticle (ultrafine) titanium dioxide pigments and stabilisers on the photooxidative stability of water based acrylic and isocyanate based acrylic coatings. Polymer Degradation and Stability. 78(3):467-78.

Alsalleeh F, Williams S, Jaber H (2016). Interaction of *Candida albicans* with periodontal ligament fibroblasts limits biofilm formation over elastomer silicone disks. Archives of oral biology. 63:47-52.

Andres CJ, Haug SP, Munoz CA, Bernal G (1992). Effects of environmental factors on maxillofacial elastomers: Part I--Literature review. Journal of Prosthetic Dentistry 68(2):327-330.

Aziz T, Waters M, Jagger R (2003a). Development of a new poly(dimethylsiloxane) maxillofacial prosthetic material. Journal of Biomedical Materials Research Part B, Applied Biomaterials 65(2):252-261.

Aziz T, Waters M, Jagger R (2003b). Analysis of the properties of silicone rubber maxillofacial prosthetic materials. Journal of Dentistry 31(1):67-74.

Bahadur S, Gong D (1992). The role of copper compounds as fillers in the transfer and wear behavior of polyetheretherketone. Wear 154(1):151-165.

Barnhart GW (1960). A new material and technic in the art of somato-prosthesis. Journal of Dental Research 39(4):836-844.

Beatty M, Mahanna G, Jia W (1999). Ultraviolet radiation-induced color shifts occurring in oil-pigmented maxillofacial elastomers. Journal of Prosthetic Dentistry 82(4):441-446.

Beatty MW, Mahanna GK, Dick K, Jia W (1995). Color changes in dry-pigmented maxillofacial elastomer resulting from ultraviolet light exposure. Journal of Prosthetic Dentistry 74(5):493-498.

Bellamy K, Limbert G, Waters MG, Middleton J (2003). An elastomeric material for facial prostheses: synthesis, experimental and numerical testing aspects. Biomaterials 24(27):5061-5066.

Bulbulian AH (1942). Congenital and postoperative loss of the ear: Reconstruction by prosthetic method. Journal of the American Dental Association 29(9): 1161-1168.

Cantor R, Webber R, Stroud L, Ryge G (1969). Methods for evaluating prosthetic facial materials. Journal of Prosthetic Dentistry 21(3):324-332.

Carvalho AL, Nishimoto IN, Califano JA, Kowalski LP (2005). Trends in incidence and prognosis for head and neck cancer in the United States: a site-specific analysis of the SEER database. International Journal of Cancer 114(5): 806-816.

Chalian VA, Phillips RW (1974). Materials in maxillofacial prosthetics. Journal of Biomedical Materials Research 8(4 Pt 2):349-363.

Chandra J, Kuhn DM, Mukherjee PK, Hoyer LL, McCormick T, Ghannoum MA (2001). Biofilm formation by the fungal pathogen *Candida albicans*: development, architecture, and drug resistance. Journal of Bacteriology 183(18):5385-5394.

Chandra J, Mukherjee PK, Ghannoum MA (2008). In vitro growth and analysis of Candida biofilms. Nature Protocols 3(12):1909-1924.

Chen MS, Udagama A, Drane JB (1981). Evaluation of facial prostheses for head and neck cancer patients. Journal of Prosthetic Dentistry 46(5):538-544.

Cottin H, Gazeau M, Doussin J, Raulin F (2000). An experimental study of the photodegradation of polyoxymethylene at 122, 147 and 193 nm. Journal of Photochemistry and Photobiology 135(1):53-64.

Craig RG, Koran A, Yu R, Spencer J (1978). Color stability of elastomers for maxillofacial appliances. Journal of Dental Research 57(9-10):866-871.

Cushing BL, Kolesnichenko VL, O'Connor CJ (2004). Recent advances in the liquid-phase syntheses of inorganic nanoparticles. Chemical Reviews 104(9): 3893-3946.

Denry I, Kelly JR (2008). State of the art of zirconia for dental applications. Dental Materials 24(3):299-307.

Dion I, Bordenave L, Lefebvre F, Bareille R, Baquey C, Monties JR, Havlik P (1994). Physico-chemistry and cytotoxicity of ceramics. Journal of Materials Science: Materials in Medicine 5(1): 18-24.

Dorjnamjin D, Ariunaa M, Shim YK (2008). Synthesis of silver nanoparticles using hydroxyl functionalized ionic liquids and their antimicrobial activity. International journal of molecular sciences 9(5): 807-820.

El Goresy A, Chen M, Dubrovinsky L, Gillet P, Graup G (2001). An ultradense polymorph of rutile with seven-coordinated titanium from the Ries crater. Science 293(5534): 1467-1470.

Eleni PN, Krokida M, Polyzois G, Gettleman L, Bisharat GI (2011). Effects of outdoor weathering on facial prosthetic elastomers. Odontology / the Society of the Nippon Dental University 99(1):68-76.

Fang S, Yimin Z, Longquan S, Jingguang P. (2006). The test of the mechanical properties of SY-28, SY-20 and MDX-4-4210 silicone elastomers. Journal of US-China Medical Science 3:36–40.

Feng QL, Wu J, Chen GQ, Cui FZ, Kim TN, Kim JO (2000). A mechanistic study of the antibacterial effect of silver ions on Escherichia coli and Staphylococcus aureus. Journal of Biomedical Materials Research 52(4):662-668.

Firtell DN, Donnan ML, Anderson CR (1976). Light-weight RTV silicone for maxillofacial prostheses. Journal of Prosthetic Dentistry 36(5):544-549.

Flörke OW, Graetsch HA, Brunk F, Benda L, Paschen S, Bergna HE, Roberts W, Welsh W, Libanati C, Ettlinger M, Kerner D, Maier M, Meon W, Schmoll R, Gies H, Schiffmann D (2008). Silica. Ullmann's Encyclopedia of Industrial Chemistry. Bochum, Federal Republic of Germany, 422-424.

Frogley M, Ravich D, Wagner H (2003). Mechanical properties of carbon nanoparticle-reinforced elastomers. Computer Science Technology 63(11):1647-1654.

Gary JJ, Huget EF, Powell LD (2001). Accelerated color change in a maxillofacial elastomer with and without pigmentation. Journal of Prosthetic Dentistry 85(6):614-620.

Gary JJ, Smith CT (1998). Pigments and their application in maxillofacial elastomers: a literature review. Journal of Prosthetic Dentistry 80(2):204-208.

Gijsman P, Hennekens J, Janssen K (1994). Comparison of UV degradation chemistry in accelerated (xenon) aging tests and outdoor tests (II). Polymer Degradation and Stability 46:63-74.

Goiato MC, Haddad MF, Sinhoreti MA, dos Santos DM, Pesqueira AA, Moreno A (2010). Influence of opacifiers on dimensional stability and detail reproduction of maxillofacial silicone elastomer. Biomedical Engineering Online 9(1):85.

Goldberg AJ, Craig RG, Filisko FE (1978). Polyurethane elastomers as maxillofacial prosthetic materials. Journal of Dental Research 57(4):563-569.

Golden JH, Deng H, Disalvoa FJ, Frechet JM, Thompson PM (1995). Monodisperse metal clusters 10 angstroms in diameter in a polymeric host: the "monomer as solvent' approach. Science 268(5216):1463-1466.

Gonzales J, Chao E, Kai-Nan A (1978). On physical and mechanical behavior of polyurethane formulations used for facial prostheses. Journal of Prosthetic Dentistry 39(3):307-318.

Gunay Y, Kurtoglu C, Atay A, Karayazgan B, Gurbuz CC (2008). Effect of tulle on the mechanical properties of a maxillofacial silicone elastomer. Journal of Dental Materials 27(6):775-779.

Han Y, Kiat-amnuay S, Powers JM, Zhao Y (2008). Effect of nano-oxide concentration on the mechanical properties of a maxillofacial silicone elastomer. Journal of Prosthetic Dentistry 100(6):465-473.

Han Y, Zhao Y, Xie C, Powers JM, Kiat-amnuay S (2010). Color stability of pigmented maxillofacial silicone elastomer: effects of nano-oxides as opacifiers. Journal of Dentistry 38(Suppl 2):e100-105.

Hatamleh MM, Watts DC (2010). Effect of extraoral aging conditions on color stability of maxillofacial silicone elastomer. Journal of Prosthodontics 19(7): 536-543.

Hay RJ (1999). The management of superficial candidiasis. Journal of the American Academy of Dermatology 40(6 Pt 2):S35-42.

Herrera M, Carrion P, Baca P, Liebana J, Castillo A (2000). In vitro antibacterial activity of glass-ionomer cements. Microbios 104(409):141-148.

Jani RM, Schaaf NG (1978). An evaluation of facial prostheses. Journal of Prosthetic Dentistry 39(5):546-550.

Karayazgan B, Gunay Y, Evlioglu G (2003). Improved edge strength in a facial prosthesis by incorporation of tulle: a clinical report. Journal of Prosthetic Dentistry 90(6):526-529.

Kazanjian V, Rowe A, Young H (1932). Prosthesis of the Mouth and Face. Journal of Dental Research 12(5):651-693.

Keyf F (2002). Change in a maxillo-facial prosthesis material effecting from environmental factors: a clinical report. Journal of Biomaterials Applications 16(4):259-266.

Khan AA, Khan A, Inamuddin (2007). Preparation and characterization of a new organic-inorganic nano-composite poly-o-toluidine Th(IV) phosphate: Its analytical applications as cation-exchanger and in making ion-selective electrode. Talanta 72(2):699-710.

Khanna PK, Singh N, Charan S (2007). Synthesis of nano-particles of anatase-TiO2 and preparation of its optically transparent film in PVA. Materials Letters 61(25):4725-4730.

Kiat-amnuay S, Beerbower M, Powers JM, Paravina RD (2009). Influence of pigments and opacifiers on color stability of silicone maxillofacial elastomer. Journal of Dentistry 37(Suppl 1):e45-50.

Kiat-Amnuay S, Mekayarajjananonth T, Powers JM, Chambers MS, Lemon JC (2006). Interactions of pigments and opacifiers on color stability of MDX4-4210/type A maxillofacial elastomers subjected to artificial aging. Journal of Prosthetic Dentistry 95(3):249-257.

Kiat-amnuay S, Waters PJ, Roberts D, Gettleman (2008). Adhesive retention of silicone and chlorinated polyethylene for maxillofacial prostheses. Journal of prosthetic dentistry 99(6): 483-488.

Kiat-amnuay S, Lemon JC, Powers JM (2002). Effect of opacifiers on color stability of pigmented maxillofacial silicone A-2186 subjected to artificial aging. Journal of Prosthodontics 11(2): 109-116.

Kim JS, Kuk E, Yu KN, Kim JH, Park SJ, Lee HJ, et al. (2007). Antimicrobial effects of silver nanoparticles. Nanomedicine 3(1):95-101.

Koran A, Yu R, Powers JM, Craig RG (1979). Color stability of a pigmented elastomer for maxillofacial appliances. Journal of Dental Research 58(5):1450-1454.

Koran A, Craig RG (1975). Dynamic mechanical properties of maxillofacial materials. Journal of Dental Research 54(6): 1216-1221.

Kuhn DM, Chandra J, Mukherjee PK, Ghannoum MA (2002). Comparison of biofilms formed by *Candida albicans* and Candida parapsilosis on bioprosthetic surfaces. Infection and immunity 70(2): 878-888.

Kumamoto CA (2002). Candida biofilms. Current Opinion in Microbiology. 5(6):608-11.

Lemon JC, Kiat-amnuay S, Gettleman L, Martin JW, Chambers MS (2005). Facial prosthetic rehabilitation: preprosthetic surgical techniques and biomaterials. Current Opinion In Otolaryngology & Head and Neck Surgery 13(4):255-262.

Li P, Li J, Wu C, Wu Q, Li J (2005). Synergistic antibacterial effects of β-lactam antibiotic combined with silver nanoparticles. Nanotechnology 16(9):1912.

Liu G, Li Y, Yan F, Zhao Z, Zhou L, Xue Q (2005). Effect of nanoscale SiO2 and TiO2 as the fillers on the mechanical properties and aging behavior of linear low-density polyethylene/low-density polyethylene blends. Journal of Polymers and the Environment 13(4):339-348.

Longo VM, Picon FC, Zamperini C, Albuquerque AR, Sambrano JR, Vergani CE, Machado AL, Andrés J, Hernandes AC, Varela JA, Longo E (2013). Experimental and theoretical approach of nanocrystalline TiO 2 with antifungal activity. Chemical Physics Letters, 577, pp.114-120.

Lontz JF (1968). Static and dynamic stress considerations in the design and use of polymeric materials in prosthetic applications. Annals of the New York Academy of Sciences 146(1): 166-192.

Lontz JF, SCHWEIGE JW, Burger AW (1974, January). Modifying stress-strain profiles of polysiloxane elastomers for improved maxillofacial conformity. Journal of Dental Research 53: 277-277.

Lughi V, Sergo V (2010). Low temperature degradation-aging of zirconia: a critical review of the relevant aspects in dentistry. Dental Materials 26(8):807-820.

Maiti M, Bhattacharya M, Bhowmick A (2008). Elastomer nanocomposites. Rubber Chemistry and Technology 81(3):384-469.

Malghe YS, Prabhu RC, Raut RW (2009). Synthesis, characterization and biological activities of mixed ligand Zr(IV) complexes. Acta Poloniae Pharmaceutica 66(1):45-50.

Mohite UH, Sandrik JL, Land MF, Byrne G (1994). Environmental factors affecting mechanical properties of facial prosthetic elastomers. International Journal of Prosthodontics 7(5):479-486.

Mohseni G, Negahdary M, Malekzadeh R, Manoochehri J, Hadaegh A, Sayad A et al. (2012). Direct electron transfer of cytochrome c on ZrO2 nanoparticles modified glassy carbon electrode. International Journal of Electrochemical Science 7(1):7033-7044.

Monteiro DR, Gorup LF, Takamiya AS, Ruvollo-Filho AC, de Camargo ER, Barbosa DB (2009). The growing importance of materials that prevent microbial adhesion: antimicrobial effect of medical devices containing silver. International journal of antimicrobial agents 34(2): 103-110.

Morones JR, Elechiguerra JL, Camacho A, Holt K, Kouri JB, Ramírez, J T., & Yacaman, M. J. (2005). The bactericidal effect of silver nanoparticles. Nanotechnology 16(10): 2346.

Mukherjee PK, Chandra J (2004). Candida biofilm resistance. Drug Resistance Updates 7(4): 301-309.

Nikawa H, Yamamoto T, Hayashi S, Nikawa Y (1994). Growth and/or acid production of *Candida albicans* on soft lining materials in vitro. Journal of Oral Rehabilitation 21(5):585-594.

Örtorp A, Kihl ML, Carlsson GE (2009). A 3-year retrospective and clinical follow-up study of zirconia single crowns performed in a private practice. Journal of dentistry 37(9): 731-736.

Panáček A, Kolář M, Večeřová R, Prucek R, Soukupová J, Kryštof V, Hamal P, Zbořil R, Kvítek L (2009). Antifungal activity of silver nanoparticles against Candida spp. Biomaterials. 30(31):6333-40.

Paravina RD, Majkic G, Del Mar Perez M, Kiat-Amnuay S (2009). Color difference thresholds of maxillofacial skin replications. Journal of Prosthodontics: Official Journal of the American College of Prosthodontists 18(7):618-625.

Pigno M, Goldschmidt M, Lemon J, (1994) The efficacy of antifungal agents incorporated into a facial prosthetic silicone elastomer. Journal of Prosthetic Dentistry, 71, 295.

Polyzois GL (1999). Color stability of facial silicone prosthetic polymers after outdoor weathering. Journal of Prosthetic Dentistry 82(4):447-450.

Polyzois GL, Tarantili PA, Frangou MJ, Andreopoulos AG (2000). Physical properties of a silicone prosthetic elastomer stored in simulated skin secretions. Journal of prosthetic dentistry. 83(5):572-7.

Pospisil J, Pilar J, Billingham NC, Marek A, Horak Z, Nespurek S (2006). Factors affecting accelerated testing of polymer photostability. Polymer Degradation and Stability 91:417–22.

Rabek JF (2012). Polymer photodegradation: mechanisms and experimental methods. Springer Science & Business Media.

Rai M, Yadav A, Gade A (2009). Silver nanoparticles as a new generation of antimicrobials. Biotechnology Advances 27(1): 76-83.

Ramage G, Walle KV, Wickes BL, López-Ribot JL (2001). Standardized method for in vitro antifungal susceptibility testing of *Candida albicans* biofilms. Antimicrobial Agents and Chemotherapy. 45(9):2475-9.

Rao K, Mahesh K, Kumar S (2005). A strategic approach for preparation of oxide nanomaterials. Bulletin of Materials Science 28(1):19-24.

Rimondini L, Cerroni L, Carrassi A, Torricelli P (2002). Bacterial colonization of zirconia ceramic surfaces: an in vitro and in vivo study. International Journal of Oral and Maxillofacial Implants 17(6):793-798.

Rothon R (Ed.) (2003). Particulate-filled polymer composites. iSmithers Rapra Publishing. Shrewsbury, UK, 489-490.

Sampers J (2002). Importance of weathering factors other than UV radiation and temperature in outdoor exposure. Polymer Degradation and Stability. 76:455–65.

Shah G, Winter R (1996). Effect of bimodality on tear properties of silicone networks. Macromolecular Chemistry and Physics 197(7):2201-2208.

Sinha SK, Briscoe BJ (2009). Polymer Tribology. Imperial College Press. London, UK 418-422.

Sweeney WT, Fischer TE, Castleberry DJ, Cowperthwaite GF (1972). Evaluation of improved maxillofacial prosthetic materials. Journal of Prosthetic Dentistry 27(3):297-305.

Tang E, Cheng G, Pang X (2006). Synthesis of nano ZnO/poly(methylmethacrylate) composite microsphere through emulsion polymerization and its UV-shielding property. Colloid and Polymer Science 284(4):422-428.

Thompson JY, Smith R, Stoner BR, Piascik JR (2011). Adhesion/cementation to zirconia and other non-silicate ceramics: Where are we now? Dental Materials 27(1):71-82.

Thostenson ET, Ren Z, Chou TW (2001). Advances in the science and technology of carbon nanotubes and their composites: a review. Composites Science and Technology 61(21):1899-1912.

Tran NH, Scarbecz M, Gary JJ (2004). In vitro evaluation of color change in maxillofacial elastomer through the use of an ultraviolet light absorber and a hindered amine light stabilizer. Journal of Prosthetic Dentistry 91(5):483-490.

Udagama A (1987). Urethane-lined silicone facial prostheses. Journal of Prosthetic Dentistry 58(3):351-354.

Watson PS, Pontefract HA, Devine DA, Shore RC, Nattress BR, Kirkham J, et al. (2005). Penetration of fluoride into natural plaque biofilms. Journal of Dental Research 84(5):451-455.

Watson S, Beydoun D, Scott J, Amal R (2004). Preparation of nanosized crystalline TiO2 particles at low temperature for photocatalysis. Journal of Nanoparticle Research 6(2): 193-207.

Wichmann M, Sumfleth J, Gojny F, Quaresimin M, Fielder B, Schulte K (2006). Glass-fibre-reinforced composites with enhanced mechanical and electrical properties - benefits and limitations of a nanoparticle modified matrix. Engineering Fracture Mechanics 73(16):2346-2359.

Xia Y, Zhang F, Xie H, Gu N (2008). Nanoparticle-reinforced resin-based dental composites. Journal of Dentistry 36(6): 450-455.

Xu AW, Gao Y, Liu HQ (2002). The preparation, characterization, and their photocatalytic activities of rare-earth-doped TiO_2 nanoparticles. Journal of Catalysis 207(2): 151-157.

Yamanaka M, Hara K, Kudo J (2005). Bactericidal actions of a silver ion solution on Escherichia coli, studied by energy-filtering transmission electron microscopy and proteomic analysis. Applied and Environmental Microbiology 71(11): 7589-7593.

Yang H, Zhu S, Pan N (2004). Studying the mechanisms of titanium dioxide as ultraviolet-blocking additive for films and fabrics by an improved scheme. Journal of Applied Polymer Science. 92(5):3201-10.

Yu B, Ahn JS, Lim JI, Lee YK (2009). Influence of TiO_2 nanoparticles on the optical properties of resin composites. Dental Materials 25(9): 1142-1147.

Zarone F, Russo S, Sorrentino R (2011). From porcelain-fused-to-metal to zirconia: clinical and experimental considerations. Dental Materials 27(1):83-96.

Zheng Y, Zheng Y, Ning R (2003). Effects of nanoparticles SiO_2 on the performance of nanocomposites. Materials Letters 57(19):2940-2944.